Technical Paper by A.L. Li and R.K. Rowe

INFLUENCE OF CREEP AND STRESS-RELAXATION OF GEOSYNTHETIC REINFORCEMENT ON EMBANKMENT BEHAVIOUR

ABSTRACT: The effects of viscous behaviour of geosynthetic reinforcement on both the short-term and long-term performance of basally reinforced embankments over inviscous soft foundations are investigated. The construction of embankments reinforced with both viscous reinforcement and inviscous reinforcement is numerically simulated to identify the magnitude of creep and stress-relaxation of reinforcement under both limit-state and working stress conditions and the consequent effects on the stability and deformations of the system. The effects of viscoelastic properties of four reinforcement products made of polyester, polypropylene, and polyethylene are examined. It is shown that the viscous behavior of geosynthetic reinforcement can decrease the short-term stability, and the creep of geosynthetic reinforcement can significantly magnify the long-term shear deformations of the foundation soil. The isochronous stiffness can reasonably represent the mobilized reinforcement stiffness at the end of construction. The mobilized reinforcement stiffness and force are examined and the design considerations are discussed.

KEYWORDS: Reinforced embankment, Geosynthetic reinforcement, Creep, Viscoelasticity, Soft soil, Stability.

AUTHORS: A.L. Li, Postdoctoral Fellow, Department of Civil Engineering, Queen's University, Kingston, Ontario, Canada K7K 3N6, Telephone: 1/613-533-6000, Ext. 77558, Telefax: 1/613-533-2128; E-mail: li@civil.queensu.ca; and R.K. Rowe, Professor, Vice Principal (Research), Queen's University, Kingston, Ontario, Canada K7K 3N6, Telephone: 1/613-533-6933, Telefax: 1/613-533-6934, E-mail: kerry@civil.queensu.ca. Corresponding author: R.K. Rowe.

PUBLICATION: *Geosynthetics International* is published by the Industrial Fabrics Association International, 1801 County Road B West, Roseville, Minnesota 55113-4061, USA, Telephone: 1/612-222-2508, Telefax: 1/612-631-9334. *Geosynthetics International* is registered under ISSN 1072-6349.

DATE: Original manuscript submitted 20 March 2001, revised version received 3 July 2001, and accepted 6 July 2001. Discussion open until 1 January 2002.

REFERENCE: Li, A.L. and Rowe, R.K., 2001, "Influence of Creep and Stress-Relaxation of Geosynthetic Reinforcement on Embankment Behaviour", *Geosynthetics International*, Vol. 8, No. 3, pp. 233-270.

1 INTRODUCTION

It has been shown that geosynthetic reinforcement materials made of polymers, typically polyester (PET), polypropylene (PP), and polyethylene (PE), are all susceptible to creep to some extent (McGown et al. 1982; Greenwood and Myles 1986; Jewell and Greenwood 1988; Leshchinsky et al. 1997). The mechanical behaviour of geosynthetics depends on a number of factors, such as the type of polymer, polymer structure, manufacturing process, loading conditions, and soil environment (McGown et al. 1982; Christopher et al. 1986; den Hoedt 1986; Greenwood 1990; Koerner et al. 1993; Cazzuffi et al. 1997). Generally, the creep rate of PE is greater than that of PP, which is greater than that of PET (den Hoedt 1986). The stress-strain behaviour of a geosynthetic is also the function of strain rates (Shrestha and Bell 1982; Rowe and Ho 1986; Bathurst and Cai 1994; Nothdurft and Janardhanam 1994; Boyle et al. 1996) and ambient temperature (Wrigley 1987; Jewell and Greenwood 1988; Bush 1990; Koerner et al. 1993; Thornton et al. 1998; Wrigley et al. 1999).

The viscoelastic nature of geosynthetics may influence the performance of reinforced soil structures. With respect to the creep deformations and creep rupture of geosynthetic reinforcement, the long-term performance is of most concern for permanent structures. Recommendations for selecting the long-term allowable strength for reinforced soil structures (especially for reinforced slopes and walls) have been made by a number of investigators (e.g., Bonaparte and Berg 1987, Jewell and Greenwood 1988, Allen 1991, and Leroueil and Rowe 2001). A few researchers have shown the importance of considering creep characteristics of geosynthetic reinforcement to interpret time-dependent behaviour of soil walls (e.g., Lopes et al. 1994, Helwany and Wu 1995, and Sawicki 1999). However, there is a paucity of literature dealing with the potential impact of reinforcement creep on the behaviour of reinforced embankments on soft foundations.

The present paper investigates the behaviour of embankments reinforced using typical geosynthetic materials manufactured from PE, PP, or PET, constructed over inviscous soft foundation soils. The potential influence of viscous behaviour of geosynthetic reinforcement on both the short-term and long-term performance of embankments is examined. The factors examined include viscoelastic properties of reinforcement, construction rate, and different foundation soil profiles. Particular attention is given to the behaviour of reinforcement during and after embankment construction.

2 GEOSYNTHETIC REINFORCEMENT MODELLING

2.1 Constitutive Modelling of Geosynthetic Reinforcement

Various models have been proposed to model the creep behaviour of geosynthetics. These have included: rheological models (e.g., Shrestha and Bell 1982, Zhang and Moore 1997a,b, Sawicki and Kazimierowicz-Frankowska 1998, and Soong and Koerner 1998); viscoplastic models (e.g., Zhang and Moore 1997a,b); power functions (Kabir 1988; Perkins 2000); and polynomial functions (Ling et al. 1992; Helwany and

Wu 1992). However, not all models can predict both the short-term and long-term creep of geosynthetics. It has been shown that a multi-Kelvin model can describe much of both short-term and long-term viscoelastic strains of geosynthetic materials (Zhang and Moore 1997a; Soong and Koerner 1998). The advantage of the multi-Kelvin model is that it can be formulated so that only a few material constants are needed and the number of Kelvin-chain models can be easily chosen as necessary to model creep over different time periods. The model adopted in the present paper is based on the nonlinear viscoelastic model proposed by Zhang and Moore (1997a). This model is composed of a nonlinear independent spring with a series of Kelvin elements. Each Kelvin element is composed of a spring and a dashpot in parallel.

The total strain, ε, is the sum of the elastic strain, ε^e and the viscous strain, ε^v. Therefore, the total strain rate, $\dot{\varepsilon}$, is given by:

$$\dot{\varepsilon} = \dot{\varepsilon}^e + \dot{\varepsilon}^v \tag{1}$$

where: $\dot{\varepsilon} = \dot{\sigma}/E_0$; σ= tensile stress (i.e., the tensile load for a geosynthetic reinforcement problem); and E_0 = modulus (i.e., the stiffness for geosynthetic reinforcement) of the independent spring, which is the function of the tensile stress as following:

$$E_0 = a_0 \exp(-a_1 \sigma^3) \tag{2}$$

where a_0 and a_1 are material constants.

The viscous strain rate, $\dot{\varepsilon}^v$, is represented by:

$$\dot{\varepsilon}^v = \sum_i^n \{\sigma/(E_i \tau_i) - \varepsilon_i^v/\tau_i\} \tag{3}$$

where: n = number of Kelvin elements; $\tau_i = \eta_i/E_i$ = retardation time; and E_i and η_i = spring modulus (i.e., the stiffness for geosynthetic reinforcement) and the dashpot viscosity of the i^{th} Kelvin element, respectively. The following equations are proposed to deduce the number of material constants:

$$E_i = \alpha^{i-1} E_1 \tag{4}$$

$$\tau_i = \beta^{i-1} \tau_1 \tag{5}$$

where E_1 and τ_1 are the material constants.

The total of seven material constants are a_0, a_1, α, β, E_1, τ_1, and n. The finite element formulation of the viscoelastic problem was derived based on the method proposed by Zienkiewicz (1977), which is similar to that for the incremental plasticity theory.

2.2 Simulation of Geosynthetic Reinforcement Creep Tests

A uniaxial formulation of the proposed constitutive model for the reinforcement was

implemented into a finite element program AFENA (Carter and Balaam 1990). Based on laboratory creep test data, finite element creep simulations were conducted to back-calculate the viscoelastic model parameters for four typical geosynthetic reinforcement products, namely: (1) a high density polyethylene (HDPE) geogrid, G1 (Leshchinsky et al. 1997); (2) a high density polyethylene geogrid, G2 (data courtesy of Tensar Earth Technologies Inc.); (3) a woven polypropylene (PP) geotextile, G3 (Greenwood 1990); and (4) a woven polyester (PET) geotextile, G4 (Greenwood 1990). The mechanical properties are given in Table 1.

Table 2 gives the back-calculated viscoelastic parameters from the creep simulations. Figure 1 compares the calculated strains with measured strains in the reinforcement at different times under a sustained tensile load. It is evident that the viscoelastic model closely simulates the creep behaviour of these geosynthetics for the time and stress range considered (i.e., at 30 to 40% of the ultimate strength, T_{ult}). This stress range corresponds to a typical range of design values for geosynthetic reinforcement. Figure 1 also shows the creep strains in reinforcement predicted based on the proposed model up to 10^5 hours (approximately 11.6 years). The creep rates of these geosynthetics follow the order: G1 (PE) > G2 (PE) > G3 (PP) > G4 (PET). The total strain of product G1 at 40% of the ultimate load increases from 2.9% at the end of loading (at 6 seconds) to 11.7% at 10^5 hours giving a creep strain of 8.8%. However, the long-term creep strain of product G4, under a sustained load of 47% of the ultimate strength, is less than 1%. It is worth mentioning that the short-term performance of the reinforcement is critical to

Table 1. Properties of the four geosynthetic reinforcement products examined.

Designated symbol	Physical properties of the geosynthetic materials				
	Reinforcement type	Polymer type	Manufacturing process	Strength, T_{ult} (kN/m)	Stiffness, J_t (kN/m)
G1	Geogrid	HDPE	PSD[(a)]	72	850
G2	Geogrid	HDPE	PSD	166	1940
G3	Geotextile	PP	Woven	186	1578
G4	Geotextile	PET	Woven	200	1736

Note: (a) PSD = punched, sheet drawn; T_{ult} and J_t are the ultimate strength and secant stiffness at 5% strain, respectively, measured from wide-width tensile tests at a constant strain rate of 10%/minute.

Table 2. The viscoelastic model parameters.

Designated symbol	Material constant						
	a_0 (kN/m)	a_1 (m/kN)	α	β	E_1 (kN/m)	τ_1 (hour)	n
G1	1,050	7.0×10^{-6}	1	10	3,000	0.02	9
G2	2,200	4.0×10^{-7}	1.1	10	6,300	0.05	9
G3	1,700	4.0×10^{-7}	0.99	10	9,800	0.03	9
G4	1,800	2.0×10^{-7}	1.2	10	60,000	0.05	7

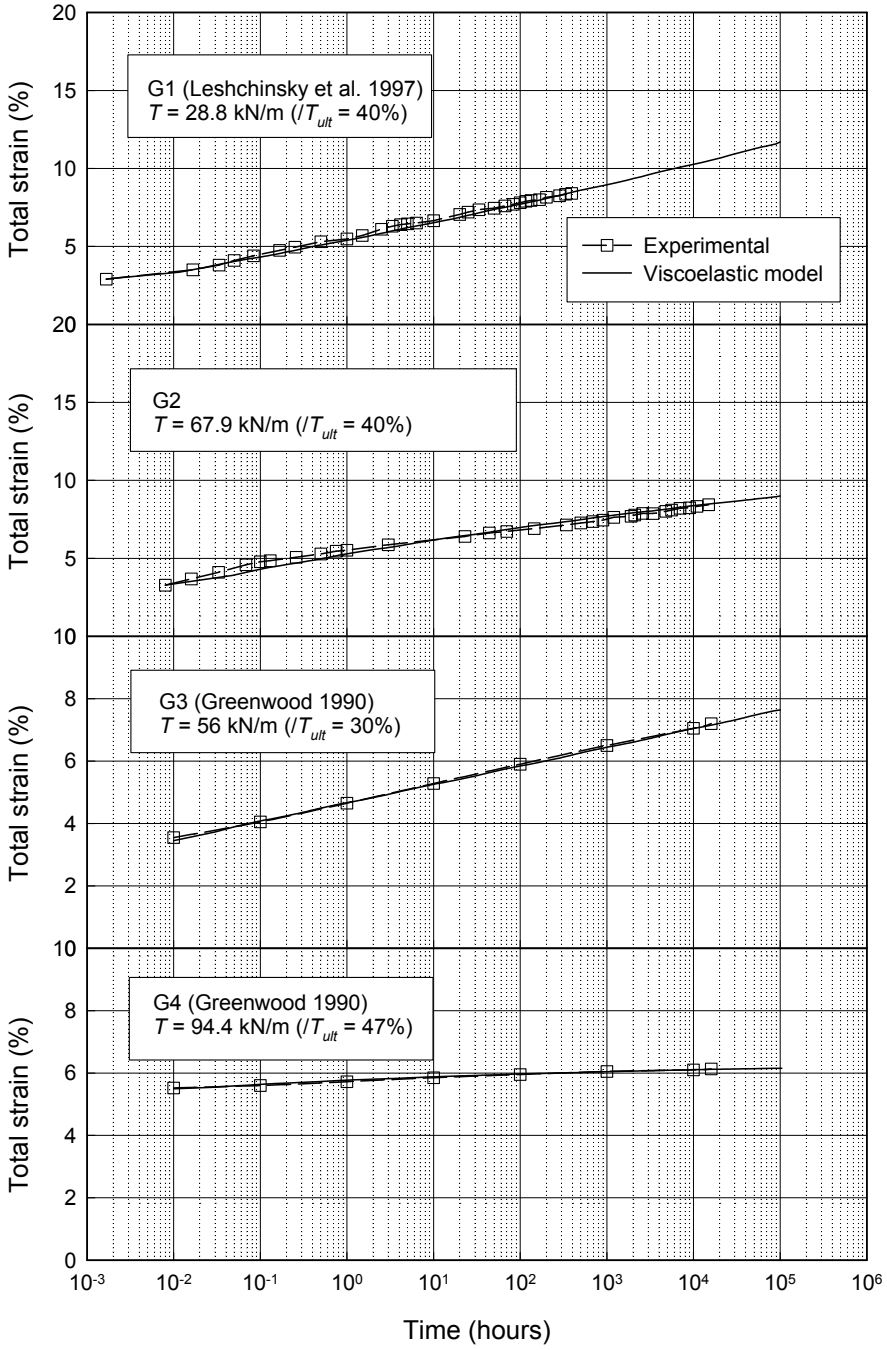

Figure 1. The measured and calculated creep strains of the four geosynthetic reinforcement products.

embankment stability since the foundation examined in the present paper will have significant strength gain due to consolidation 10 years after construction.

The proposed model can also describe the nonlinear tensile behaviour of geosynthetics. Figure 2 shows simulation results of tensile tests for G2 at different strain rates. The calculated curve at 10%/minute strain rate with $a_1 = 2.5 \times 10^{-7}$ m/kN agrees well with the measured data from an ASTM D 4596 wide-width tensile test at 10%/minute strain rate up to failure. However, $a_1 = 4 \times 10^{-7}$ m/kN was adopted since the predicted tensile force agrees very well with the measured force for the strain range of 4 to 6% (which is a range of common interest) as shown in Figure 2. Based the model parameters of product G2 calibrated using experimental creep and tensile data, the stress-strain response of product G2 at strain rates of 10 and 0.02%/hour has been predicted (Figure 2). Figure 2 shows that the strain rate has a significant influence on the stiffness. Cheok (1985) (as referenced by Nothdurft and Janardhanam (1994)) also shows the same trend for a similar HDPE geosynthetic product.

3 FINITE ELEMENT MODELLING AND MODEL PARAMETERS

A typical four-lane highway embankment with 2H:1V side slopes that overlies a 15 m-thick soft cohesive deposit underlain by a relatively permeable layer was considered. The finite element mesh, with a total of 1,594 linear strain triangular elements and

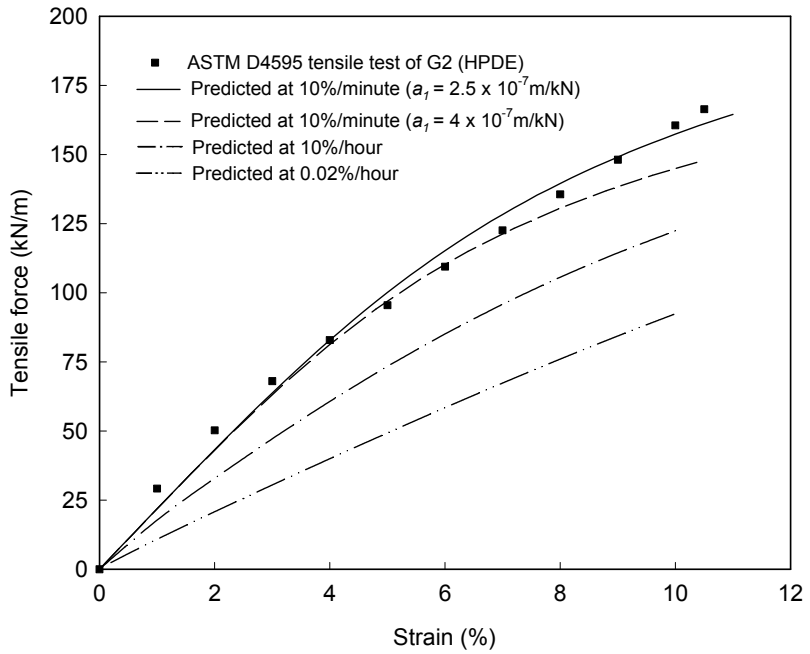

Figure 2. ASTM D 4595 tensile test and predicted results for geosynthetic G2.

3,516 nodes, was used to discretize the embankment and foundation soils. Two-noded bar elements were used for the reinforcement and two-noded joint elements were used for both the embankment fill-reinforcement interface and the embankment fill-foundation interface. The centerline of the embankment and the far field lateral boundary at a 100 m distance from the centreline were taken to be smooth and rigid. The bottom of the finite element mesh was assumed to be rough and rigid, and zero excess pore pressures were assigned to the nodes along the bottom boundary line. Embankment construction was simulated by turning on the gravity of the fill in 0.75 m-thick lifts at a rate corresponding to the embankment construction rate, *CR*.

3.1 Foundation Soil Properties

A modified version of the finite element program AFENA (Carter and Balaam 1990) was adopted in the analysis. An elasto-plastic elliptical cap model (Chen and Mizuno 1990; Rowe and Li 1999) fully coupled with Biot consolidation theory (Biot 1941) is used to describe the yielding behaviour of the soft foundation soil. In the overconsolidated state, the soil behaves elastically with an elastic bulk modulus, *K*, and shear modulus, *G*, given by:

$$K = \frac{1+e}{\kappa}\,\sigma'_m \tag{6}$$

$$G = \frac{3(1-2\nu')K}{(1+2\nu')} \tag{7}$$

where: σ'_m = mean effective stress; e = void ratio; κ = slope of the e - ln(σ'_m) curve in the overconsolidated range; and ν = Poisson's ratio. In the normally consolidated state, the yield function is defined as:

$$F(\sigma_{ij}, \sigma_y) = (\sigma'_m - l)^2 + 2J_2R^2 - (\sigma_y - l)^2 = 0 \tag{8}$$

where: J_2 = second invariant of the deviatoric stress tensor; R = aspect ratio in $\sigma'_m - \sqrt{2J_2}$ space; l = mean effective stress corresponding to the centre of the ellipse; and σ_y = intercept of the ellipse with σ'_m axis. The strain hardening function is defined as:

$$\partial\sigma_y = \frac{1+e}{\lambda-\kappa}\sigma_y\,\partial\,\varepsilon_v^p \tag{9}$$

where: λ = compression index in e - ln(σ_m) space; and ε_v^p = plastic volumetric strain. Failure is defined by the Drucker-Prager failure envelope:

$$f(\sigma_{ij}) = \sqrt{2J_2} - M\sigma'_m - c_K = 0 \tag{10}$$

where: M = slope of the Drucker-Prager failure envelope in $\sigma'_m - \sqrt{2J_2}$ space (M = $M_{O/C}$ for the overconsolidated stress range and $M = M_{N/C}$ for normally consolidated stress range); and c_K = cohesion intercept.

The hydraulic conductivity of soft clays was taken to be a function of void ratio:

$$k_v = k_{vo} \exp\left(\frac{e - e_o}{C_k}\right) \tag{11}$$

where: k_{vo} = reference hydraulic conductivity; C_k = hydraulic conductivity change index; and e_o = reference void ratio. The anisotropy of the hydraulic conductivity is considered by using the ratio of the hydraulic conductivity in the vertical and horizontal directions, k_h / k_v.

Two inviscous soft foundation soil profiles, denoted as Soils A and B, examined in the present paper have the initial vertical effective stress and preconsolidation profiles as shown in Figure 3. Soil A has a liquid limit of 76% and plasticity index of 40%, and Soil B has a liquid limit of 48% and plasticity index of 30%. Both Soils A and B were slightly overconsolidated with an *OCR* of 1.1 to 2.6 and 1.1 to 2.9, respectively, below the first two metres (Figures 3a and 3b). Soil B, with a 2 m crust, has a higher preconsolidation pressure, σ_p', than Soil A. The initial void ratio and unit weight are taken to be 2.0 to 2.5 and 14.7 to 15.6 kN/m^3 for Soil A, and 1.3 to 1.5 and 16.5 to 16.9 kN/m^3 for Soil B, respectively. Both the elliptical cap and hydraulic conductivity parameters are summarised in Table 3. Using these parameters, for the Soil A profile, the undrained shear strength s_{uo} at the surface was calculated to be 5 kPa and the rate of

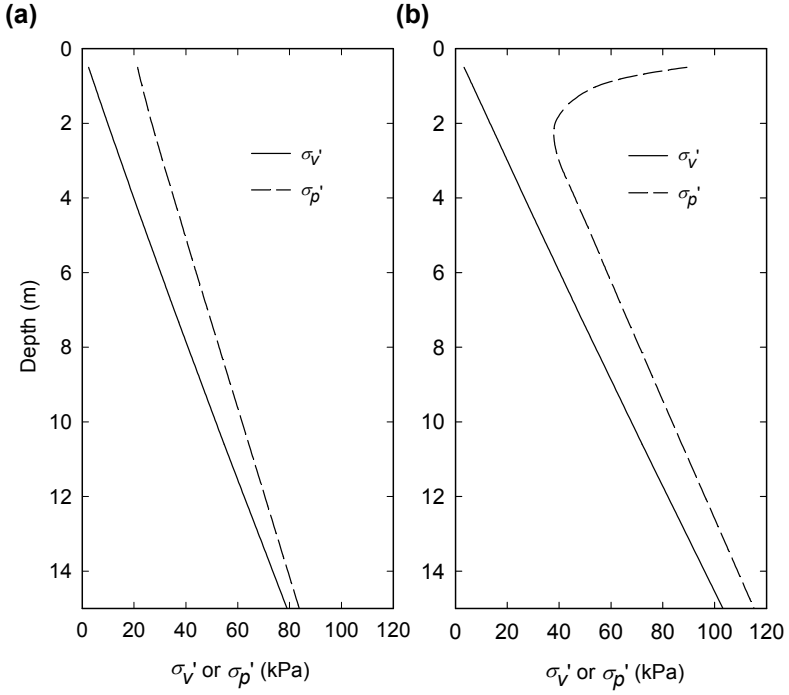

Figure 3. Preconsolidation pressure and initial vertical effective stress profiles: (a) Soil A; (b) Soil B.

Table 3. The foundation soil model parameters.

Parameters	Soil A	Soil B
Failure envelope, $M_{N/C}$ (ϕ')	0.874 (27°)	0.91 (28°)
Failure envelope, $M_{O/C}$	0.63	0.75
Aspect ratio, R	0.70	1.25
Compression index, λ	0.30	0.15
Recompression index, κ	0.03	0.025
Coefficient of earth pressure at rest, K_0'	0.60	0.60
Poisson's ratio, ν'	0.35	0.30
Bulk unit weight, γ (kN/m^3)	15.2	16.7
Initial void ratio, e_o	2.03 to 2.5	1.31 to 1.5
Hydraulic conductivity parameters		
k_{vo} (m/s)	1×10^{-9}	1×10^{-9}
e_o	2.5	1.5
C_k	0.5	0.5
k_h / k_v	3	3

increase in undrained strength with depth was 1.5 kPa/m. For the Soil B profile, s_{uo} was 20 kPa at the surface, decreased to 10 kPa at a 2 m depth, and then increased with depth at a rate of 2.0 kPa/m. The undrained shear strength profiles of Soils A and B are similar to those of the natural soft clay deposits reported by Litwinowicz et al. (1994) and Chai and Bergado (1993), respectively.

3.2 Embankment Fill Parameters

An elasto-perfectly-plastic model with a Mohr-Coulomb failure surface and a non-associated flow rule (Davis 1968) was adopted for the granular embankment fill. It was assumed to be a purely frictional granular soil with a peak friction angle $\phi' = 37°$, dilatancy angle $\psi = 6°$, and a unit weight $\gamma = 20$ kN/m^3. The nonlinear elastic stiffness of the granular soil was modelled using Janbu's equation (Janbu 1963), i.e.

$$(E/P_a) = K_s(\sigma_3/P_a)^m \tag{12}$$

where: E = Young's modulus of the soil; P_a = atmospheric pressure; σ_3 = minor principal stress; K_s and m = material constants selected to be 300 and 0.5, respectively.

3.3 Interface Parameters

The geosynthetic reinforcement was considered using the one-dimensional viscoelastic model as described in Section 2.1. The interaction between the soil mass and the reinforcement was modelled by introducing soil-reinforcement interface elements with strength governed by Mohr-Coulomb failure criterion (Rowe and Soderman 1987).

The frictional angle of the fill-reinforcement interface was assumed to be 37°. The fill-foundation interface had the same shear strength as that of the foundation soil at the ground surface.

4 ANALYSIS RESULTS

Typical geosynthetic reinforcement has an allowable strain ranging between 4 and 7% (deduced using allowable strength and short-term stiffness from the "2000 Specifier's Guide" (Industrial Fabrics Association International 1999)). The reinforcement strain of 5% in the short-term may potentially increase to a performance limit strain of 10% in the long-term (McGown et al. 1984; Wrigley et al. 1999) for some HDPE geogrids. In the present paper, construction of embankments, reinforced using the four types of geosynthetic products shown in Table 1 to heights limited by an allowable reinforcement strain of approximately 5% at the end of construction (EOC), was simulated to investigate the embankment behaviour at limit state. A construction rate, *CR*, of 10 m/month was adopted except for a few analyses where the influence of construction rates is investigated. At these embankment heights, there was a contiguous failure zone in the foundation soil and, hence, without the presence of basal reinforcement, the embankment would not be stable.

4.1 Influence of Viscoelastic Behaviour of Reinforcement During Embankments Construction

To investigate the potential effect of creep and stress-relaxation of the reinforcement during construction, the finite element simulation of embankment construction using G2 reinforcement over Soils A and B was conducted. Figure 4 shows the calculated net embankment height (i.e., fill thickness minus settlement) versus fill thickness for the G2 reinforced embankments during 10- and 15-day construction periods at a constant construction rate of 10 m/month over Soils A and B, respectively. The embankment failed when the placement of the fill material caused a decrease in net embankment height. The failure height, H_f (i.e., the fill thickness at failure), was 3.38 and 4.88 m and the mobilized reinforcement strain at embankment failure, ε_f, was 5.2 and 5.3% for the embankment over Soils A and B, respectively. At the failure strain, the corresponding reinforcement force (at embankment failure) was 66 and 67 kN/m for the embankment over Soils A and B, respectively. It is evident that the mobilized force for embankment construction over both Soils A and B was significantly less than the ultimate geosynthetic strength, T_{ult} = 166 kN/m (Table 1).

Figure 4 also shows the results for embankment construction using a perfectly elastic (i.e., inviscous) reinforcement with stiffness J = 1940 kN/m, which is equal to the secant stiffness at 5% strain of G2 measured from the wide-width tensile test at a strain rate of 10%/minute. The embankment failure height, H_f, for inviscous reinforcement was 3.75 and 5.7 m and the failure strain ε_f was 5.4 and 9.4% for Soils A and B, respectively. Figure 4 indicates that the creep sensitive reinforcement G2 behaved less stiff than it would in a tensile test at a relatively fast strain rate (i.e., 10% /minute) due

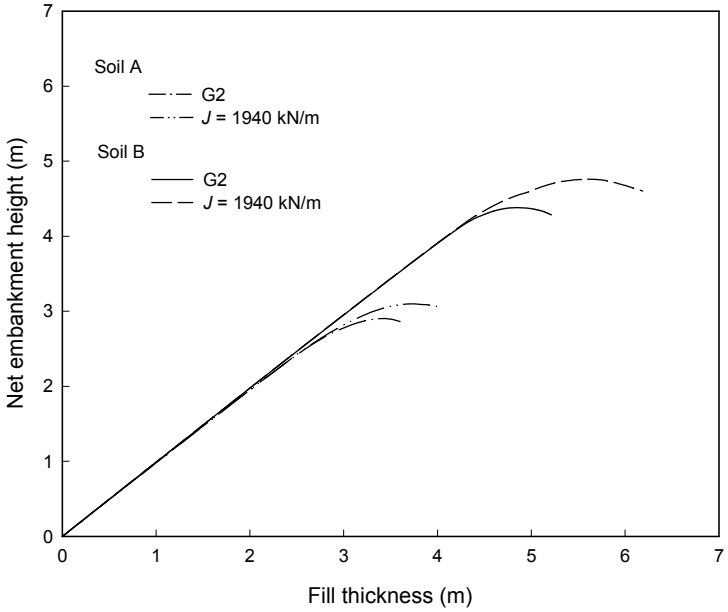

Figure 4. The variation of net embankment height with fill thickness.

to creep and stress-relaxation of the reinforcement during construction. Consequently, the viscoelastic behaviour of geosynthetic reinforcement decreased the embankment stability, as is evident by examining the failure heights shown in Figure 4.

4.2 Influence of Viscoelastic Behaviour of Reinforcement on Embankments at Limit State

4.2.1 *Time Dependent Reinforcement Strain*

Four reinforced embankments were numerically constructed over both inviscous foundation Soils A and B using reinforcement products G1, G2, G3, and G4. For an allowable reinforcement strain within 4 to 5%, developed at the end of construction, the calculated embankment height, H, was 2.82, 3.15, 3.15, and 3.5 m over Soil A and 4.48, 4.75, 4.75, and 5 m over Soil B using G1, G2, G3, and G4, respectively. Figures 5 and 6 show (solid lines) the variation of the maximum reinforcement strain with time during and after construction up to the time when 98% consolidation of the foundation soils was reached. To identify the effect of viscoelastic properties of geosynthetics, each embankment was also constructed using inviscous (linear elastic) reinforcement (dashed line) with an axial stiffness having approximately the same value of viscous reinforcement developed at the end of construction. Since the stiffness of the elastic reinforcement was selected so that the end of construction strains of both viscous and inviscous reinforcement were practically the same, the difference in the long-term rein-

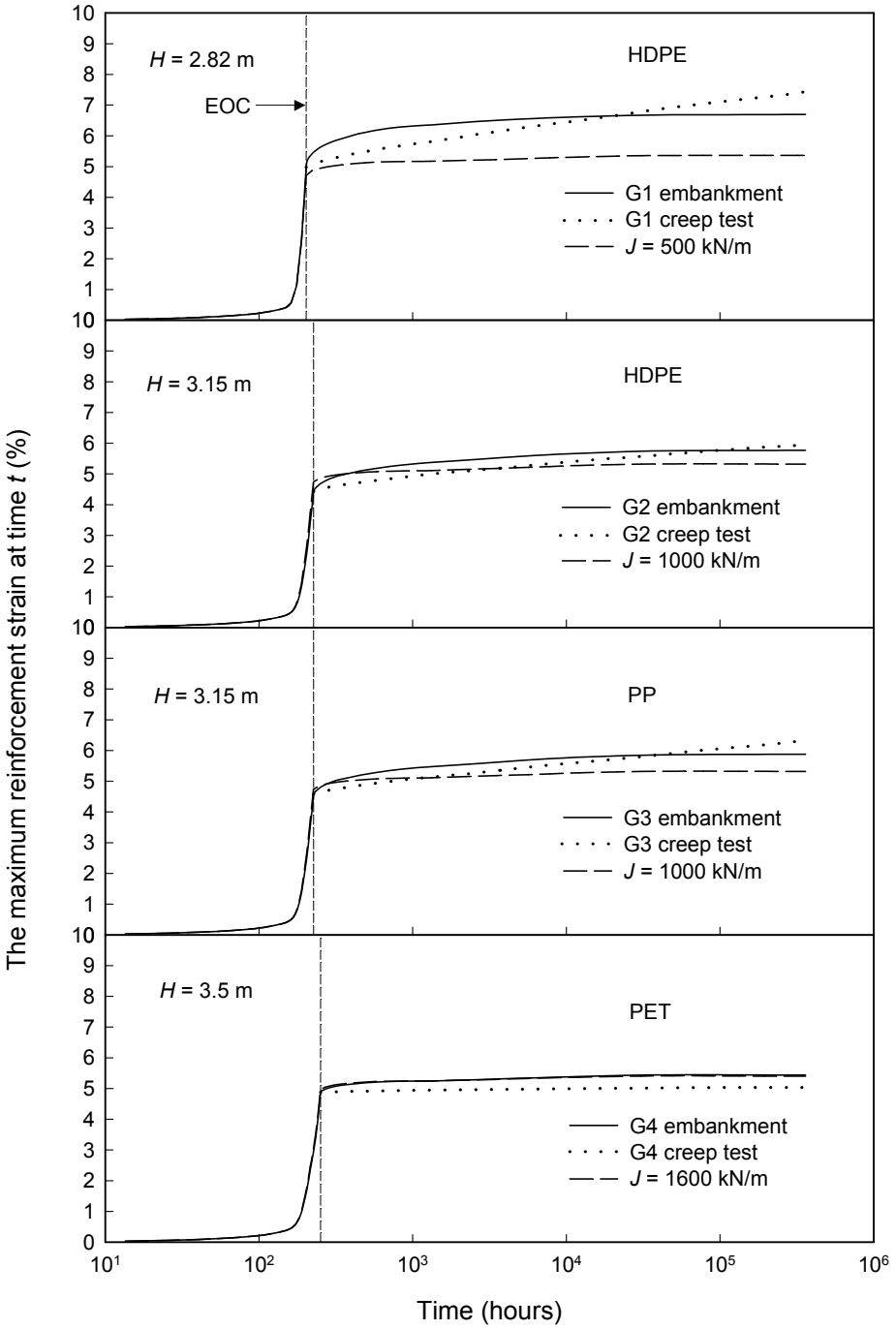

Figure 5. The variation of reinforcement strain with time for embankments over Soil A.

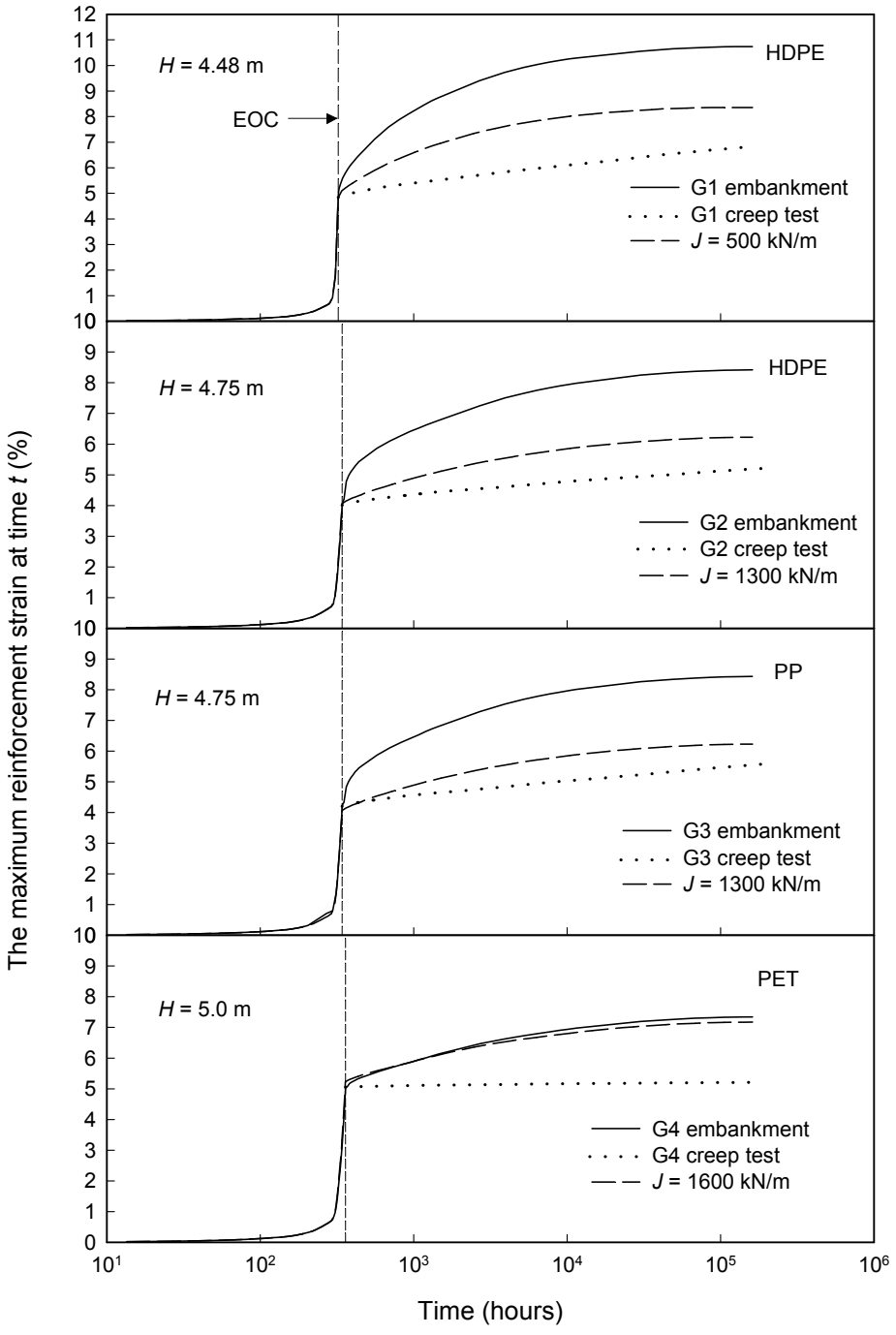

Figure 6. The variation of reinforcement strain with time for embankments over Soil B.

forcement strains was attributed to the creep of the viscous reinforcement if the mobilized force did not increase with time. This was true for embankments constructed over Soil A since the reinforcement force decreased with time (discussed in more detail in Section 4.2.2).

For embankments over Soil A (Figure 5), the HPDE geogrid, G1, reinforced embankment had the lowest fill height, but had the most reinforcement creep strain develop. The net increase of the maximum strain, between the end of construction and the time at which consolidation was 98% complete was 1.71%. The embankment reinforced with woven polyester geotextile, G4, was the highest, and there was practically no reinforcement creep strain developed. The maximum strains for reinforcement G2 and G3 at the end of construction were 4.44 and 4.55%, respectively, and the creep strain following construction until 98% consolidation was 1.36 and 1.33%, respectively. It is shown that even though the HPDE geogrid, G2, was stiffer than the woven polypropylene geotextile, G3, in terms of wide-width tensile stiffness, the time dependent reinforcement strain was very similar for a given embankment height. This is because the mobilized tensile stiffness of the reinforcement at the end of construction was affected by its viscous properties. Consequently, a higher initial stiffness and the more viscous nature of G2 resulted in an end-of-construction stiffness approximately the same as that of G3, which had a lower initial stiffness but a less viscous response.

Also, shown (dotted line) in Figure 5 are results from a simulated creep test of each reinforcement, wherein the reinforcement was loaded to the same maximum strain level as the reinforcement in the embankment at the end of construction, over a period equal to the embankment construction time. It was then allowed to creep under the sustained load. As can be seen from Figure 5, the isolated creep test results tend to underpredict the early strains and overpredict the later strains for embankments over Soil A. This suggests that the creep of reinforcement after embankment construction was dependent on the time varying interaction and stress redistribution in the embankment and foundation during consolidation.

The higher embankments that could be constructed over Soil B (Figure 6) showed the effect of creep more clearly than the lower embankments over Soil A. Reinforcement G1 exhibited the most creep strain, and reinforcement G4 exhibited the least creep strain. The maximum strain of G1 increased from 4.8% at the end of construction to 10.7% at 98% consolidation, which exceed the limit strain of 10% for a similar HPDE reinforcement reported by McGown et al. (1984) and Wrigley et al. (1999). Exceeding the "limit strain" could potentially cause creep rupture of reinforcement G1, however, the factor of safety of this embankment without reinforcement at 98% consolidation was 1.7 calculated based on the method proposed by Li and Rowe (2000). Thus, the embankment would be stable in the event of breakage of reinforcement G1.

As shown in Figure 6, the net increase of strain in G1, G2, G3, and G4 after construction was 5.9, 4.4, 4.2, and 2.3%, respectively, which was higher than that predicted by simulated creep tests. In the embankment case, the reinforcement strain increased due to the differential settlement and foundation horizontal movements during consolidation in addition to creep strains. The significant soil movements after construction (discussed in more detail in Section 4.2.3) caused further tensioning of the reinforcement, which resulted in a relatively high reinforcement strain developed

at a relatively low stiffness due to the nonlinear behaviour of the reinforcement (Figure 2). The increase in reinforcement strain after construction was more significant for the embankments over Soil B than for the embankments over Soil A because the greater applied stress, related to the higher embankments over Soil B, resulted in a greater long-term deformation and consequent straining of the reinforcement. The effect of stress redistribution and post-construction deformation is most evident for the embankment with reinforcement G4 (which experienced little creep). The synergistic effect of stress redistribution and creep is most evident for the embankment with reinforcement G1, which exhibited the greatest creep effects.

For the embankment over Soil B, the increase in strain of the viscous reinforcement after construction can be decomposed into three components, namely: the strain due to creep, which can be calculated from the creep test; the strain due to consolidation, which can be calculated from the strain of the inviscous reinforcement; and the strain due to nonlinear tensile properties, which can be calculated using mobilized force and stiffness. For example, for the 4.48 m-high, G1-reinforced embankment (Figure 6), the total increase in strain between the end of construction and 98% consolidation was 5.9%. This consisted of: a creep strain of 2.0%, calculated from the creep test simulation; a consolidation strain of 3.5%, calculated from the case with inviscous reinforcement; and a nonlinear tensile strain of 0.4%, calculated from the difference of reinforcement strain for a net increase in force of 9 kN/m (from 23.5 kN/m at EOC to the maximum of 32.5 kN/m after EOC; this is discussed in more detail in Section 4.2.2).

The predicted increase of reinforcement strain after construction shown in Figures 5 and 6 is consistent with field observations. For example, Bassett and Yeo (1988) reported the reinforcement strain increased during consolidation for a HPDE geogrid-reinforced trial embankment from 2 to 3%. Schimelfenyg et al. (1990) also reported an increase of up to 1.5% during consolidation for a 5 m-high woven geotextile reinforced dike embankment with a long-term total maximum strain of approximately 7%.

Figure 7 shows the distribution of reinforcement strain at the end of construction and at 98% consolidation for G2-reinforced embankments over Soils A and B. The increase in reinforcement strain after construction was most significant at locations below the embankment crest. It is evident that the increase in deformation with time is not uniform, and the corresponding stress redistribution gives rise, in part, to the increase in reinforcement strain shown in Figures 5 and 6.

It is evident from the cases examined in the present study that the effects of reinforcement creep even for a given reinforcement product can vary quite significantly depending on the embankment height and the characteristics of the underlying foundation soil even when creep of the foundation soil is not considered.

4.2.2 *Mobilized Reinforcement Force and Stiffness*

Figures 8 and 9 show the variation of reinforcement force with time for the embankments examined in the Section 4.2.1. The difference between the force developed in the viscous reinforcement and the force in the inviscous reinforcement was attributed to stress-relaxation of the viscous reinforcement after the end of construction for embankments over Soil A and partially attributed to stress-relaxation of the viscous

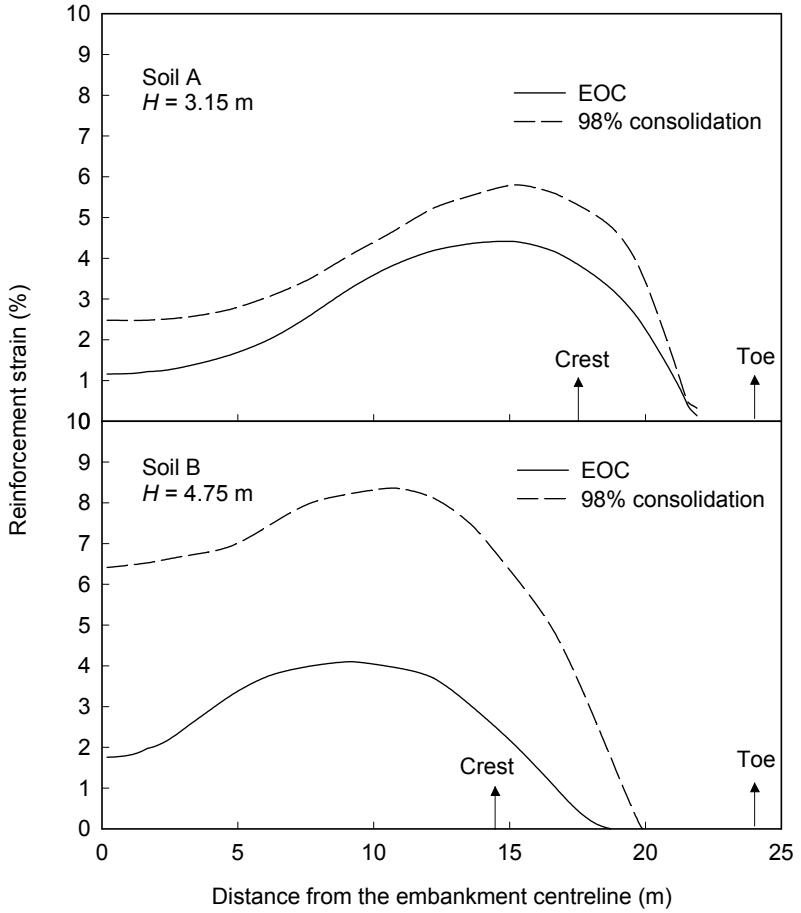

Figure 7. The distribution of reinforcement strains at the end of construction and 98% consolidation for G2-reinforced embankments over Soils A and B.

reinforcement for embankments over Soil B. It is evident that the more viscous the reinforcement the more stress-relaxation that occurred after construction. For embankments over Soil A, G1, G2, and G3 reinforcement had a noticeable decrease in reinforcement force, and G4 had practically constant force. However, all embankments over Soil B had an increase in reinforcement force due to the lateral straining of reinforcement associated with the horizontal movements in the foundation soil and differential settlement associated with consolidation as discussed in Section 4.2.1. The predicted increase of reinforcement force after construction has also been observed in field cases (e.g., Bassett and Yeo 1988 and Duncan and Schaefer 1988).

To compare the behaviour of reinforcement in the field and in the laboratory, the simulation of stress-relaxation tests was also conducted for each reinforcement prod-

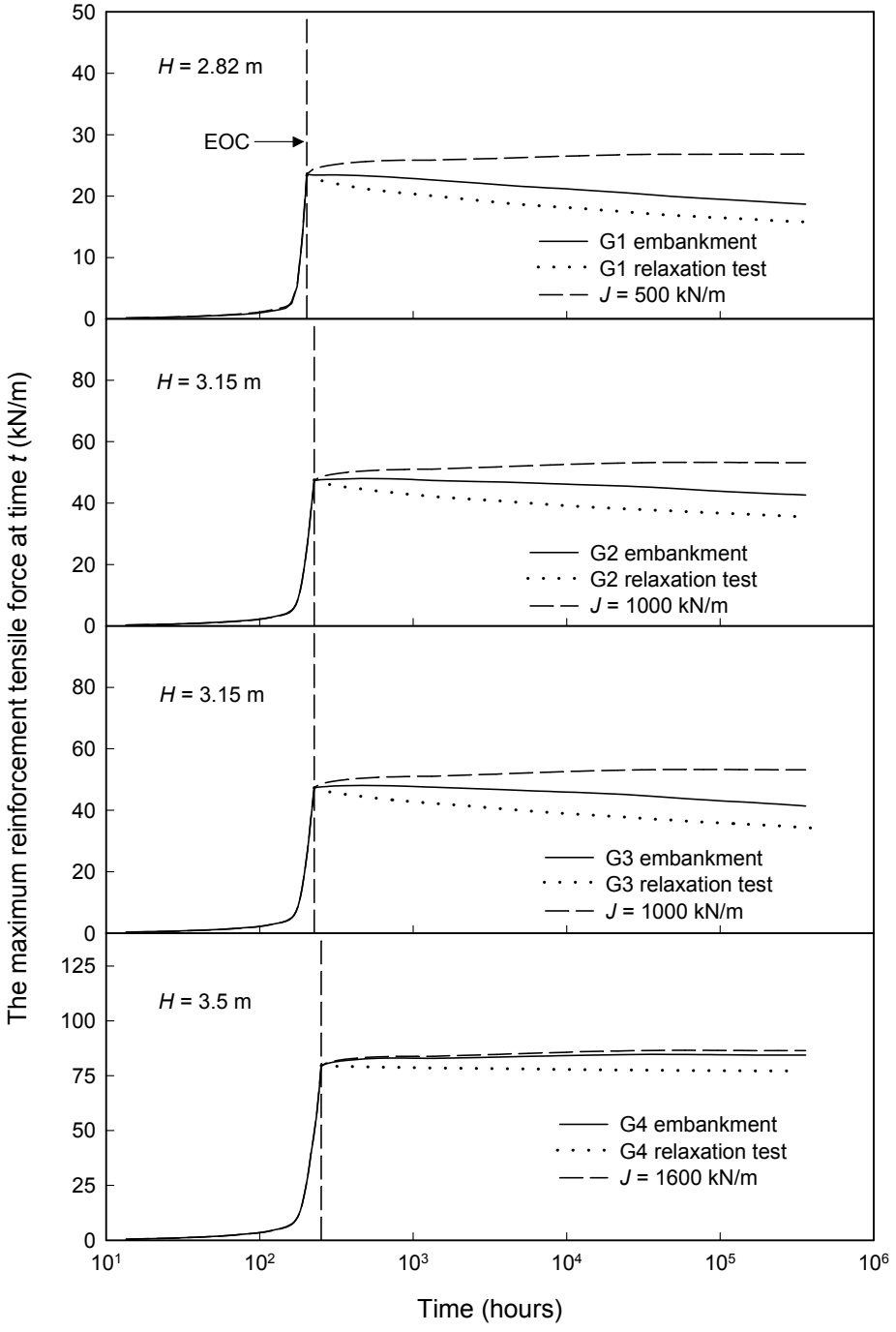

Figure 8. The variation of reinforcement force with time for embankments over Soil A.

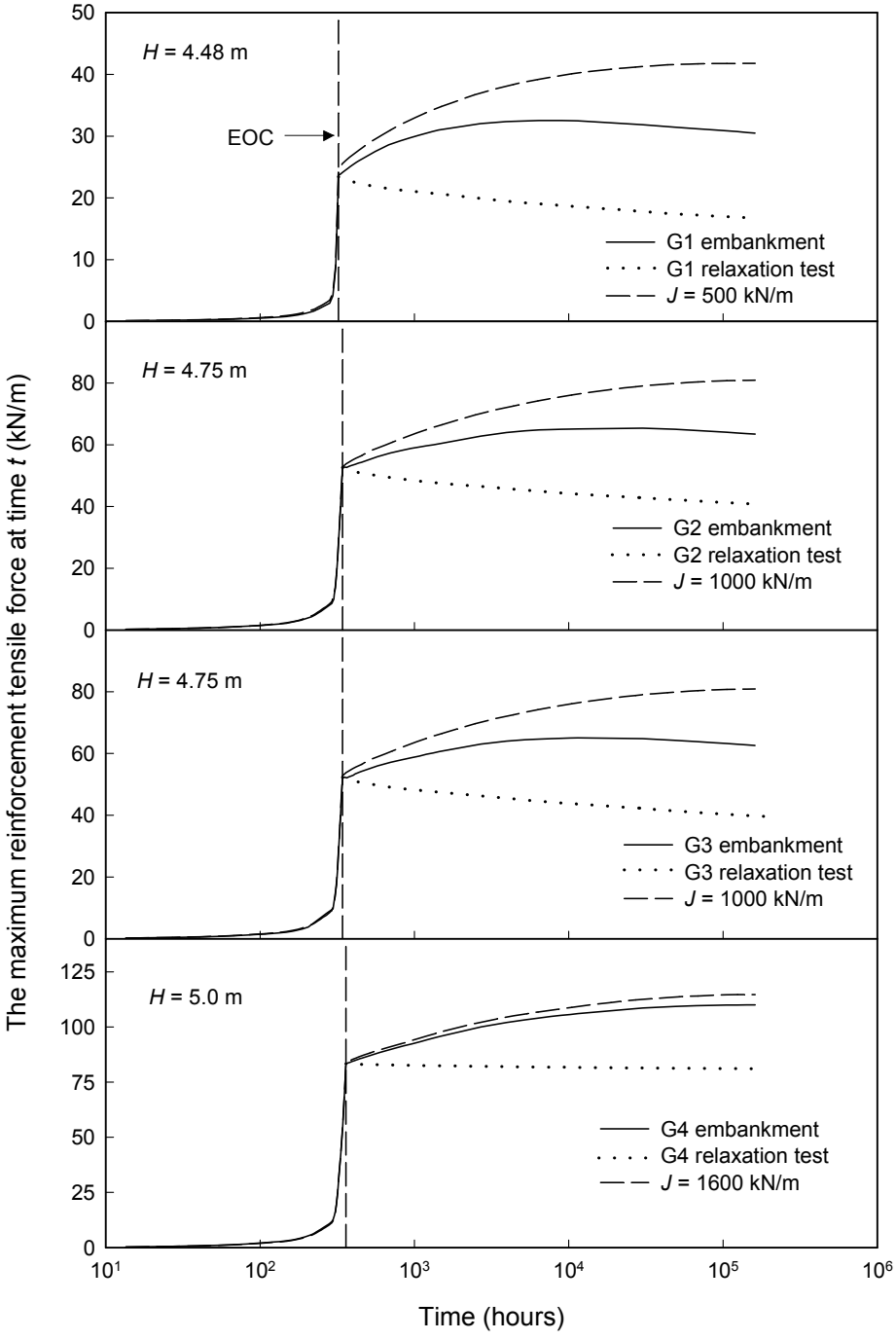

Figure 9. The variation of reinforcement force with time for embankments over Soil B.

uct. For the stress-relaxation test, the reinforcement was strained over a period equal to the construction time to the same force that was developed at the end of construction. Figures 8 and 9 show that the simulated isolated relaxation tests overpredict the stress-relaxation calculated in the embankment for all cases examined.

Based on the reinforcement force and strain developed, the mobilized reinforcement stiffness can be calculated at different times. Figures 10 and 11 compare the mobilized reinforcement stiffness (i.e., the secant stiffness at the mobilized strain) with isochronous stiffness deduced from the creep test data shown in Figure 1. In general, the mobilized stiffness decreased with time and approached very closely the isochronous stiffness in the long-term. The increase in stiffness before EOC and decrease after EOC was caused by the strain rate effect on the behaviour of the viscous reinforcement. The rapid deformations of foundation soils prior to the end of construction, due to the development of plasticity in the foundation soil, resulted in a slightly stiffer response of the reinforcement. The sharp appearance of the change is also due to the logarithmic time scale and, in fact, it is more gradual when plotted with a linear time scale.

It is evident from Figures 10 and 11 that the mobilized reinforcement stiffness at the end of construction was lower than the isochronous stiffness at the beginning of the creep test as well as being lower than the stiffness measured in a tensile test at a standard rate of 10%/minute (Table 1). The average mobilized stiffness at the end of construction for embankments over Soils A and B was 56, 60, 71, and 95% of the secant stiffness at 5% strain from the tensile test at 10%/minute at the same strain level for reinforcement G1, G2, G3, and G4, respectively. It indicates that the creep and stress-relaxation of reinforcement during embankment construction can significantly decrease the mobilized stiffness especially for the HPDE geogrid reinforcement and PP geotextile reinforcement. This is attributed to the strain rate dependence of reinforcement stiffness as shown in Figure 2 for reinforcement G2. The strain rate of 0.02%/hour (Figure 2) corresponds to the average strain rate at which reinforcement would deform during embankment construction with a construction rate of 10 m/month for the cases examined herein. At this strain rate, the force corresponding to a strain of 5%, is approximately half of the force required to mobilize the same strain at a 10%/minute strain rate. This highlights the need for care when deducing and applying tensile stiffness from standard stress-strain tests (e.g., ASTM D 4595).

To investigate the potential effect of the construction rate on the mobilization of reinforcement stiffness, two additional analyses were conducted for G1-reinforced embankments constructed over Soil A at construction rates, CR, of 2 and 30 m/month, respectively. It was found that the mobilized stiffness at EOC was significantly lower than the initial tensile stiffness for all cases. As might be expected, the stiffness at EOC for a construction rate of CR = 10 m/month was slightly higher than that for CR = 2 m/month and somewhat lower than that for CR = 30 m/month. This implies that for a given allowable strain, the force deduced based on the tensile stiffness measured at a 10%/minute strain rate is likely to be higher than the force that can be actually mobilized at the end of embankment construction at typical construction rates. This implies that the conventional stability calculation using the reinforcement force calculated from the allowable strain and short-term stiffness will overestimate the stability and/or the mobilized strain will be greater than the allowable strain. Figures 10 and 11 suggest

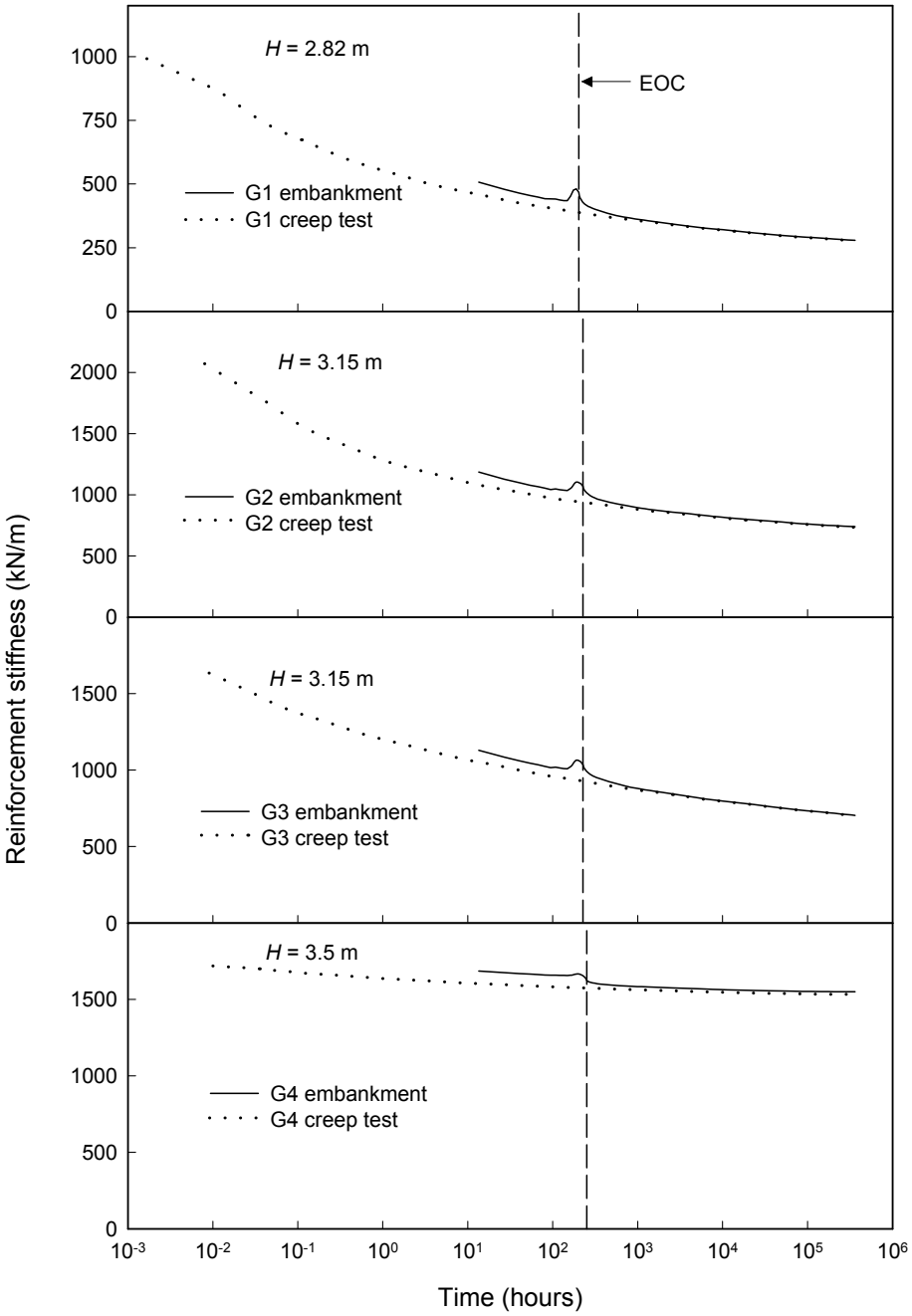

Figure 10. The variation of reinforcement stiffness with time for embankments over Soil A.

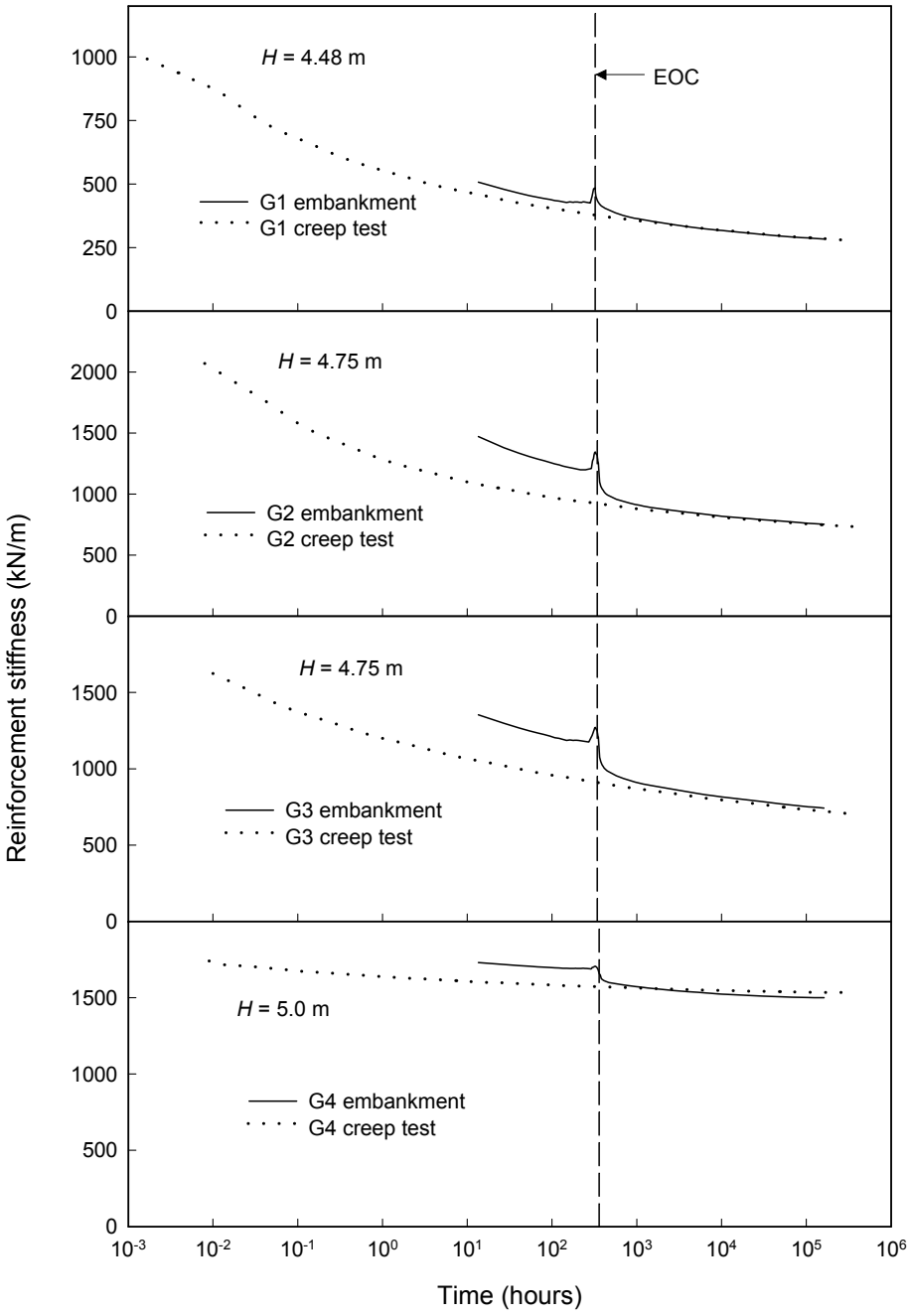

Figure 11. The variation of reinforcement stiffness with time for embankments over Soil B.

that the isochronous stiffness at the end of construction can reasonably and conservatively represent the mobilized stiffness.

4.2.3 *Foundation Deformations due to the Creep and Stress-Relaxation of Reinforcement*

Figure 12 shows the net increase in horizontal deformation after construction during consolidation below the embankment toe for both embankments with inviscous and viscous reinforcement constructed over Soil A. For the cases with inviscous reinforcement, the increase of foundation horizontal displacements after construction was related to consolidation and stress-redistribution including the Mandel-Cryer effect (Schiffman et al. 1969). The difference in horizontal deformation between the case with viscous reinforcement and the case with inviscous reinforcement can be attributed to creep and stress-relaxation of the viscous reinforcement. It is evident that the increase in horizontal deformation due to creep and stress-relaxation was significant for the cases with reinforcements G1, G2, and G3 and it was insignificant for the case with reinforcement G4. The time-dependent horizontal deformations of Soil B (Li 2000) were found to be higher than those of Soil A since the foundation Soil B experienced substantially higher compression than the foundation Soil A due to the higher embankments that could be constructed on Soil B. It was also found that the creep and stress-relaxation of reinforcement increased vertical shear deformations near the embankment toe and below the embankment crest, but had practically no effect on the settlement at the embankment centreline.

Figure 13a shows the velocity vectors induced by the 2% creep strain and 0.4% tensile strain due to nonlinear tensile properties of reinforcement G1 during consolidation for the 4.48-m high reinforced embankment over Soil B. The deformations shown in Figure 13a were obtained from the difference in deformation between the case with viscous G1 and inviscous $J = 500$ kN/m reinforcement at 98% average degree of consolidation. The length of the vector represents the relative magnitude of the creep and stress-relaxation induced deformation. The directions of the vectors indicate the rotational movement of the soils due to the shear action imposed by the embankment load. It is evident that the reinforcement creep and stress-relaxation allowed an increase in the shear deformations of the system. Figure 13b shows the contours of the increase in maximum shear strain within the foundation soil, $(\varepsilon_1 - \varepsilon_3)/2$, for the deformations shown in Figure 13a. The shape of the contours mirrors the deformation vectors in Figure 13a. With 2% reinforcement creep strain in addition to 0.4% tensile strain, the increase in maximum shear strain of the foundation soils below the embankment toe was over 8%, which was over 4 times the creep strain of the reinforcement (G1). This suggests that special care should be taken if consideration is being given to using creep-sensitive reinforcement for embankments constructed over brittle soils in addition to the recommendations made by Mylleville and Rowe (1991).

4.3 Behaviour of Reinforcement Under Working Stress Conditions

The behaviour of reinforcement under working stress conditions is examined in this

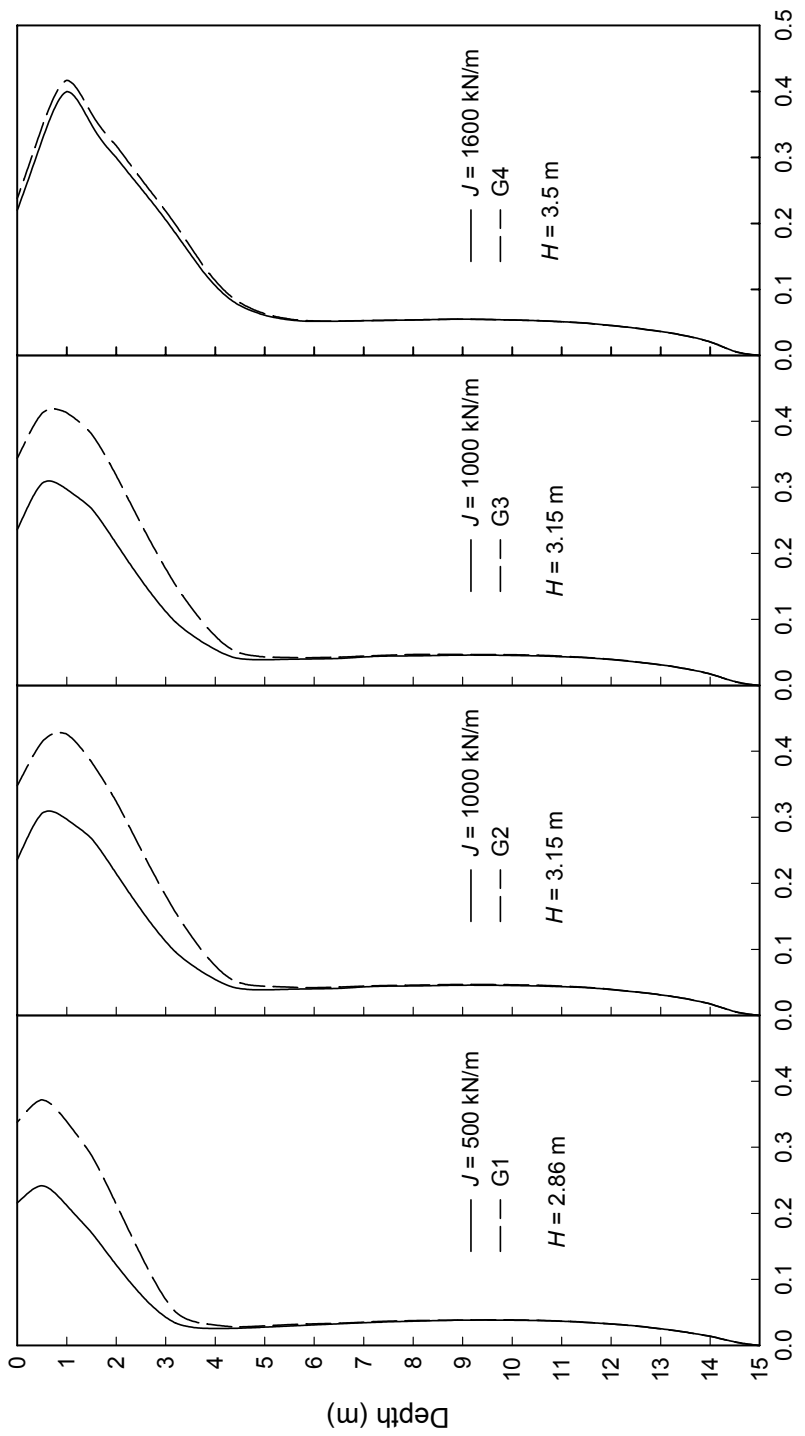

Figure 12. Change of horizontal deformations below the embankment toe between EOC and 98% consolidation for embankments over Soil A.

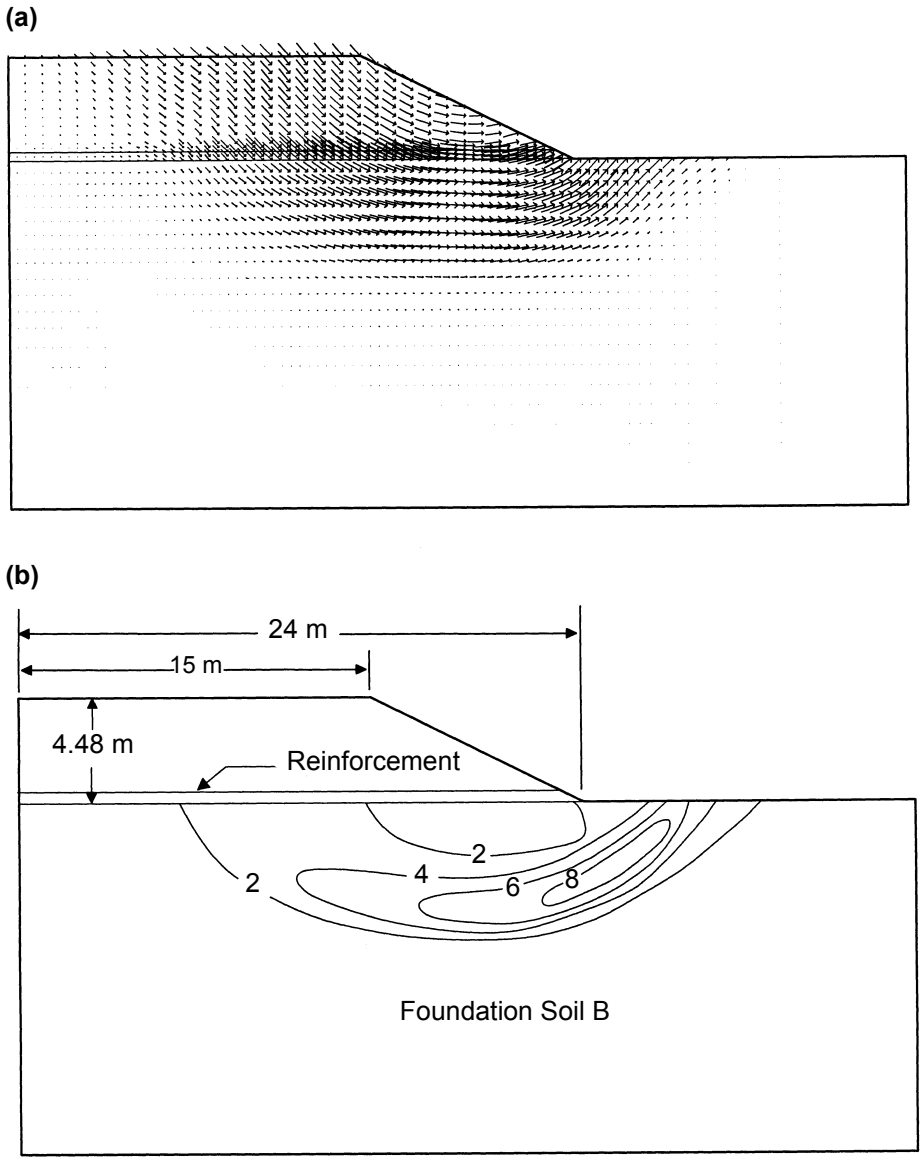

Figure 13. Deformations of foundation Soil B due to 2% creep strain and 0.4% tension strain of G1 between the end of construction and 98% consolidation under the 4.48 m-high, G1-reinforced embankment: (a) velocity vector; (b) contours of maximum shear strain (%).

section based on the limit-state design method (Becker 1996; McGown et al. 1998). The limit equilibrium program REAP (Mylleville and Rowe 1988) was used to design embankments for a limit-equilibrium ratio of 1.0 using factored soil and reinforcement

parameters (i.e., such that the factored moment resistance was equal to the over turning moment related to the factored loads). An allowable strain, ε_{all}, of 5% (which was in the range of typical allowable strains between 4 and 7% deduced from "2000 Specifier's Guide" (Industrial Fabrics Association International 1999)) was adopted. To consider the short-term viscous effect of reinforcement, the isochronous stiffness, J_i, at time equal to construction time was used except for the creep insensitive reinforcement G4. Since the stiffness from the wide-width tensile tests at a rate of 10% (denoted as J_t) is widely used (Industrial Fabrics Association International 1999), the design based on J_t was also examined. The ratio of J_t to J_i is approximately 2.1 for G1 and G2, and 1.7 for G3. This ratio is equivalent to a partial factor for the short-term creep consideration during construction. Other partial factors used are f_{c1} = 1.3 for the foundation soil undrained shear strength, f_{c2} = 1.0 for the fill-foundation interface strength, f_ϕ = 1.2 for both the embankment fill strength and reinforcement-fill interface strength parameters $\tan\phi$, and f_γ = 1.0 for the unit weight of the embankment fill.

The calculated embankment design heights, based on the limit equilibrium analysis (using REAP, Mylleville and Rowe 1988), are listed in Table 4. The construction of embankments to these design heights at a construction rate of 10 m/month over foundation Soils A and B with the real soil strength (i.e., unfactored) was numerically simulated and Figures 14 and 15 show the time-dependent maximum reinforcement strain up to 98% consolidation. For embankments constructed over both foundation soils, the reinforcement strain at the end of construction was between 0.35 and 1%, and the long-term increase of reinforcement strain ranged between 0 and 0.5% during consolidation for embankments based on both J_i and J_t. Thus, in both cases, the mobilized strain was well below the allowable strain adopted (i.e., 5%). This can be attributed to two factors: (1) the actual strength of the foundation soil was higher than the factored strength used in design; and (2) the strength gain, due to the partial consolidation during construction, increased stability. Under such working stress conditions, the embankments were stable without the additional resistance from reinforcement since the foundation

Table 4. Calculated embankment heights based on limit equilibrium analyses.

Reinforcement[a]		Embankment height (m)	
		Soil A	Soil B
G1	J_i = 400 kN/m	1.9	2.8
	J_t = 850 kN/m	2.15	3
G2	J_i = 960 kN/m	2.2	3
	J_t = 1,940 kN/m	2.55	3.45
G3	J_i = 940 kN/m	2.2	3
	J_t = 1,578 kN/m	2.4	3.3
G4	J_t = 1,736 kN/m	2.5	3.4

Note: (a) J_t = secant stiffness at 5% strain measured from wide-width tensile tests at a constant strain rate of 10%.

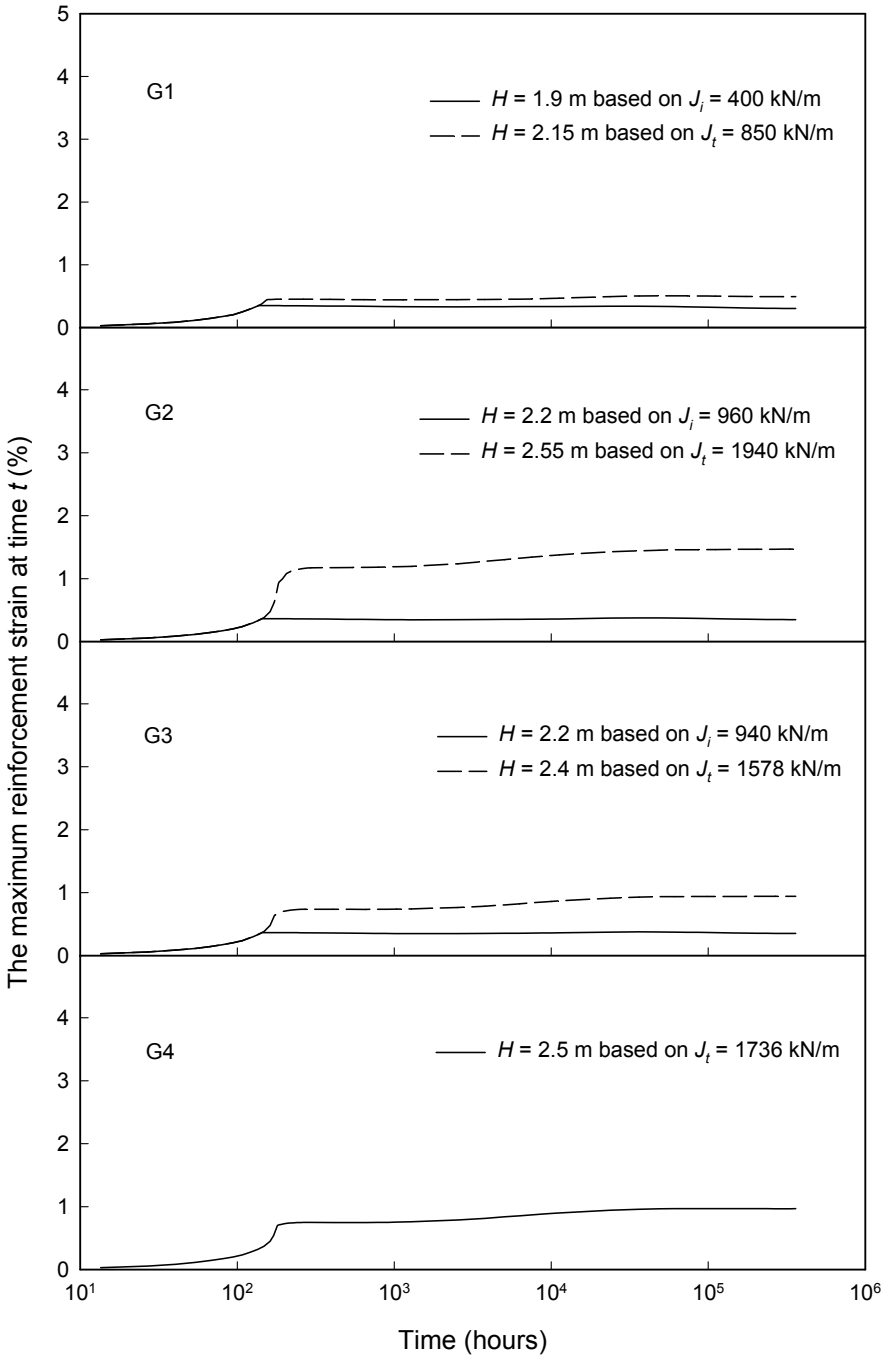

Figure 14. The variation of reinforcement strain with time for embankments over Soil A under working conditions.

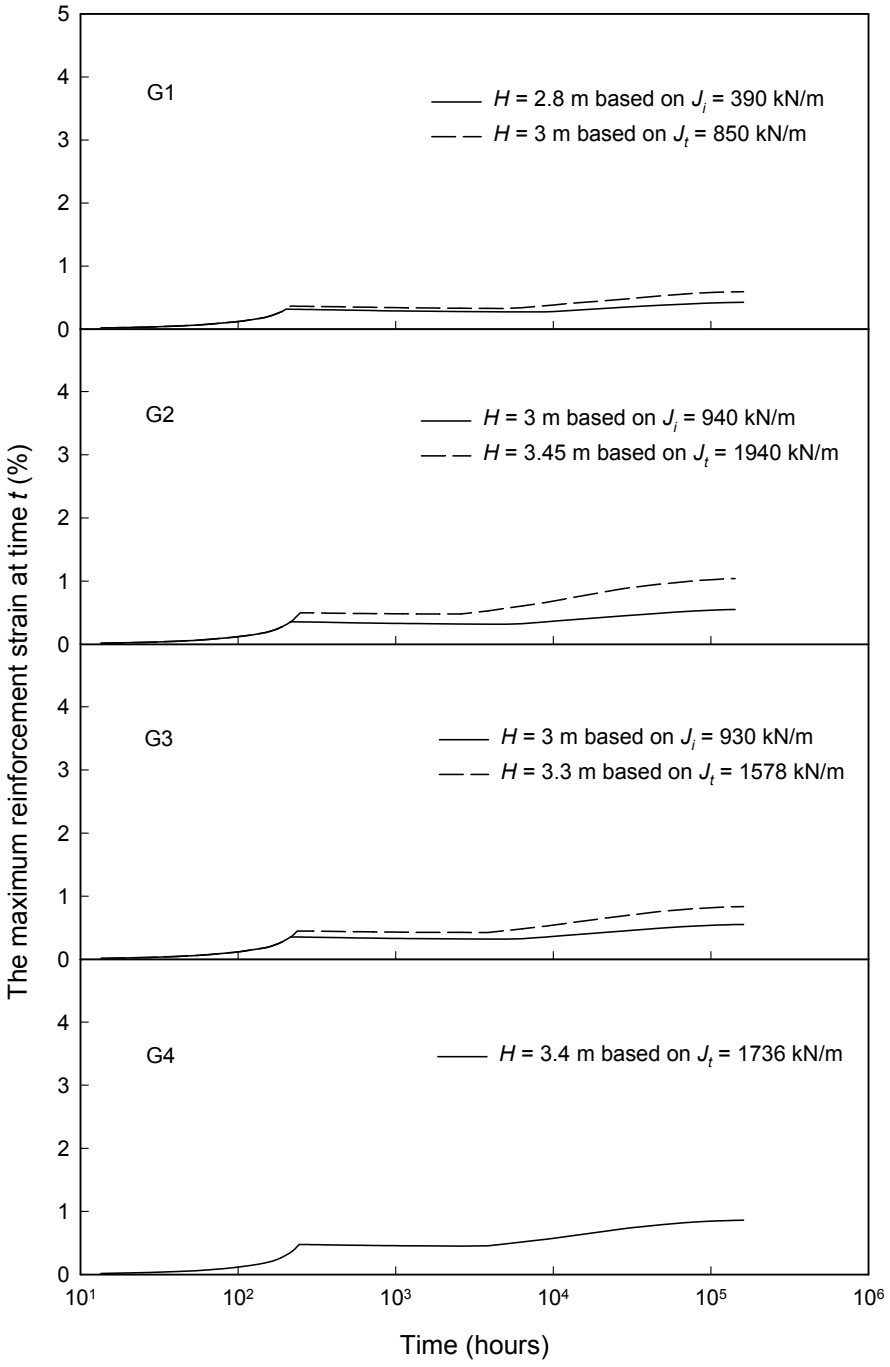

Figure 15. The variation of reinforcement stiffness with time for embankments over Soil B under working conditions.

soil strength was not fully mobilized at the end of construction and there was no contiguous plastic failure zone developed in the foundation soil below the embankment. Consequently, the mobilized strain was well below the allowable strain. This is consistent with the observation that the mobilized reinforcement strain or force in instrumented embankments was lower than the design values (Fowler and Edris, Jr. 1987; Bassett and Yeo 1988; Fritzinger 1990; Litwinowicz et al. 1994; Loke et al. 1994). However, as will be shown in Section 5, reinforcement can play a significant role if the soil conditions are not as good as anticipated and the mobilized reinforcement strains for design, based on the isochronous stiffness and tensile stiffness, can be significantly different.

The conservative assumptions made in the design discussed above also resulted in an insignificant increase in reinforcement strain during the long-term as shown in Figures 14 and 15. The slight increase of reinforcement strain after construction up to 98% consolidation for embankments designed based on J_i was also observed for the embankments constructed with inviscous reinforcement with constant stiffness being equal to the values of J_i. This indicates that there was practically no long-term creep strain developed in reinforcement when the embankments were at this working state since the deformations of the reinforcement were controlled by the foundation soil movements at the working state. This finding is different from that when the shear strength of the foundation is mobilized and the reinforcement is essential to provide stability as shown in Section 4.2.1.

5 IMPLICATIONS FOR DESIGN

It has been shown that the embankment failure height decreases due to the effects of creep and stress-relaxation of geosynthetics during embankment construction and the mobilized geosynthetic stiffness can be significantly smaller than that measured in a standard tensile test especially for polyethylene and polypropylene geosynthetics that exhibit significant viscous behaviour. Theoretically, the mobilized reinforcement force will never reach the ultimate strength, T_{ult}, measured in a standard test at a strain rate of 10%/minute if the mobilized stiffness is less than the measured stiffness J_t in such tests. This implies that the embankment design should not be directly based on the ultimate strength T_{ult}. Since the mobilized reinforcement force is dependent on the reinforcement stiffness, the embankment stability will be governed by the mobilized stiffness rather than by the ultimate reinforcement strength. However, there is not a unique value of stiffness that can be used for design since the mobilized stiffness is time dependent as shown in Figures 10 and 11. From the cases examined, it appears that the isochronous stiffness can reasonably represent mobilized stiffness at the end of embankment construction.

In light of foregoing, in order to assure the short-term stability of geosynthetic-reinforced embankments, a logical design approach would be based on the isochronous stiffness J_i and allowable strain ε_{all} of the geosynthetic reinforcement rather than the ultimate strength T_{ult} or the tensile stiffness J_t and allowable strain ε_{all}. The choice of the partial safety factor for geosynthetic viscous behaviour based on short-term

stress-strain relationships would be more reasonable than one based on long-term creep rupture of the geosynthetic since the short-term viscous effects of geosynthetics are more critical than the long-term effects as shown previously. The results from a range of conditions considered have also shown that the design based on an appropriate allowable strain and a tensile stiffness J_t (to compensate for conservative assumptions made in current practice) maybe feasible if the in situ operational undrained shear strength is indeed significantly higher than the factored design strength. In addition to creep effects, consideration should be given to the construction damage of reinforcement (Allen and Bathurst 1994, 1996).

The maximum allowable strain of reinforcement at the end of construction is limited by the serviceability constraint (Jewell and Greenwood 1988), the compatible strain (Rowe and Soderman 1985), the creep-rupture strain of reinforcement (Allen 1991; Wrigley et al. 1999), and the type of embankment fills (Holtz et al. 1997). Further research work is needed to address the choice of allowable strains for different geosynthetics and soil conditions.

To envisage how reinforced embankments would behave if the in situ operational shear strength of the foundation soil were lower than the design strength, say, equal to the factored strength, one can consider the behaviour of reinforced embankments at the limit state examined in Section 4.2 as the behaviour of embankments under working conditions. The stable behaviour of those embankments (as shown in Section 4.2) implies that the design based on isochronous stiffness J_i and allowable strain ε_{all} is safe even if the operational shear strength of the foundation soil is equal to the factored strength. For the design method based on J_t and ε_{all}, a G2-reinforced embankment was taken as an example to demonstrate the effect of uncertainty of soil strength. The design embankment height was calculated to be 3.6 m based on J_t = 19,40 kN/m and ε_{all} = 5% of reinforcement G2 if the operational strength of Soil A was assumed to be the factored strength of the foundation soil. The construction of the G2-reinforced embankment to this height resulted in a maximum reinforcement strain of 10% at end of construction, which had the same magnitude of the failure strain of geosynthetic G2 (i.e., 10.5%). It implies that the design method based on the tensile stiffness, J_t, and allowable strain (ε_{all} = 5%) may be unsafe if the operational shear strength of the foundation soil is as low as the reduced shear strength. It also implies that the direct use of the ultimate strength T_{ult} in design calculations will be also unsafe since the ultimate strength is higher than the force mobilized at the allowable strain.

As shown in Figures 14 and 15, the relatively small reinforcement strain mobilized under working conditions is attributed to conservative design assumptions associated with the mobilized soil strength and partial consolidation. In addition, a small reinforcement strain mobilized in the field can also result from a stiffer response of reinforcement in the field than in laboratory tests due to the effects of the potential low in situ temperature and soil confinement on the viscoelastic properties of geosynthetics as observed in several field cases (e.g., Litwinowicz et al. 1994, Loke et al. 1994, and Bergado et al. 1994).

6 CONCLUSIONS

The construction of embankments reinforced using both creep sensitive and creep insensitive reinforcement constructed over inviscous soft foundation soils was investigated. The time-dependent behaviour of four typical geosynthetic reinforcements (i.e., two high density polyethylene geogrids, one woven polypropylene geotextile, and one woven polyester geotextile) was examined. The creep strain after embankment construction and creep-induced foundation deformations were evaluated. The influence of viscous behaviour of reinforcement on the embankment short-term stability was identified. The following conclusions are based on the cases examined.

1. During embankment construction, viscoelastic geosynthetic reinforcement is less stiff than that interpreted from wide-width tensile tests at a standard rate of 10%/minute due to its creep and stress-relaxation during the construction period. The direct use of the short-term tensile stiffness (e.g., based on ASTM D 4595 wide-width tensile tests) leads to an overprediction of embankment design height and an underprediction of the embankment deformations. The isochronous stiffness measured from the creep tests can reasonably and conservatively represent the end of construction stiffness.
2. The creep and stress relaxation of reinforcement strain can magnify the foundation shear deformations and increase the toe and foundation lateral deformations, but had practically no influence on the settlement at the embankment centreline.
3. The reinforcement force after embankment construction may increase over a period of time when differential settlement and lateral movements of foundation soils due to consolidation are significant. This is in a stark contrast to the traditional assumption that the reinforcement force will decrease with time after construction (due to stress-relaxation).
4. Under working conditions, the creep of reinforcement was found to be insignificant due to the fact that the fill and foundation soil design strength are not fully mobilized and hence the soil is stable without the reinforcement (in conventional geotechnical terms, the reinforcement provides the "factor of safety" against failure – it is really only needed if conditions are not what was expected). Thus, the long-term reinforcement strain is significantly lower than the allowable strain as a result of the conservative design assumptions.
5. The design method, based on the isochronous stiffness at the end of construction and allowable strain of reinforcement, proved to be safe and conservative based on the cases examined.

ACKNOWLEDGEMENTS

The work reported in the present paper was funded by the Natural Sciences and Engineering Research Council of Canada. The authors wish to thank J. Han from Tensar Earth Technologies Inc. for providing the test data.

REFERENCES

Allen, T.M., 1991, "Determination of Long-Term Tensile Strength of Geosynthetics: A State-of-the-Art Review", *Proceedings of Geosynthetics '91*, IFAI, Vol. 1, Atlanta, Georgia, USA, February 1991, pp. 351-379.

Allen, T.M. and Bathurst, R.J., 1994, "Characterization of Geosynthetic Load-Strain Behavior After Installation Damage", *Geosynthetics International*, Vol. 1, No. 2, pp. 181-199.

Allen, T.M. and Bathurst, R.J., 1996, "Combined Allowable Strength Reduction Factor for Geosynthetic Creep and Installation Damage", *Geosynthetics International*, Vol. 3, No. 3, pp. 407-439.

ASTM D 4595, "*Standard Test Method for Tensile Properties of Geotextiles by the Wide-Width Strip Method*", American Society for Testing and Materials, West Conshohocken, Pennsylvania, USA.

Bassett, R.H. and Yeo, K.C., 1988, "The Behaviour of a Reinforced Trial Embankment on Soft Shallow Foundations", *Theory and Practice of Earth Reinforcement*, Yamanouchi, T., Miura, N. and Ochiai, H., Editors, Balkema, Proceedings of the International Geotechnical Symposium on Theory and Practice of Earth Reinforcement, Fukuoka Kyushu, Japan, October 1988, pp. 371-376.

Bathurst, R.J. and Cai, Z., 1994, "In-Isolation Cyclic Load-Extension Behaviour of Two Geogrids", *Geosynthetics International*, Vol. 1, No. 1, pp. 1-19.

Becker, D.E., 1996, "Eighteenth Canadian Geotechnical Colloquium: Limit States Design for Foundations. Part I. An Overview of the Foundation Design Process", *Canadian Geotechnical Journal*, Vol. 33, No. 6, pp. 956-983.

Bergado, D.T., Long, P.V., Loke, K.H., Christopher, B.R., and Delmas, P., 1994, "Geotextile Reinforcement in Full-Scale Test Embankment on Soft Ground", *Proceedings of the Fifth International Conference on Geotextiles, Geomembranes and Related Products*, Vol. 1, Singapore, September 1994, pp. 21-24.

Biot, M.A., 1941, "General Theory of Three-Dimensional Consolidation", *Journal of Applied Physics*, Vol. 12, No. 2, pp. 155-164.

Bonaparte, R. and Berg, R., 1987, "Long-Term Allowable Tension for Geosynthetic Reinforcement", *Proceedings of Geosynthetics '87*, IFAI, Vol. 1, New Orleans, Louisiana, USA, February 1987, pp. 181-192.

Boyle, S.R., Gallagher, M,. and Holtz, R.D., 1996, "Influence of Strain Rate, Specimen Length and Confinement on Measured Geotextile Properties", *Geosynthetics International*, Vol. 3, No. 2, pp. 205-225.

Bush, D.I., 1990, "Variation of Long Term Design Strength of Geosynthetics in Temperatures up to 40°C", *Proceedings of the Fourth International Conference on Geotextiles, Geomembranes and Related Products,* Balkema, Vol. 2, The Hague, Netherlands, May 1990, pp. 673-676.

Carter, J.P. and Balaam, N.P., 1990, *"AFENA - A general finite element algorithm: users manual*", School of Civil and Mining Engineering, University of Sydney,

N.S.W. 2006, Australia.

Cazzuffi, D., Ghinelli, A., Sacchetti, M., and Villa, C., 1997, "European Experimental Approach to the Tensile Creep Behaviour of High-Strength Geosynthetics", *Proceedings of Geosynthetics '97*, IFAI, Vol. 1, Long Beach, California, USA, March 1997, pp. 253-266.

Chai, J. and Bergado D.T., 1993, "Performance of Reinforced Embankment on Muar Clay Deposit", *Soils and Foundations*, Vol. 33, No. 4, pp. 1-17.

Chen, W.F. and Mizuno, E., 1990, "*Nonlinear Analysis in Soil Mechanics - Theory and Implementation*", Elsevier, New York, New York, USA, 661 p.

Christopher, B.R., Holtz, R.D., and Bell, W.D., 1986, "New Tests for Determining the In-Soil Stress-Strain Properties of Geotextiles", *Proceedings of the Third International Conference on Geotextiles*, Vol. 2, Vienna, Austria, April 1986, pp. 683-688.

Davis, E.H., 1968, "Theories of Plasticity and Failure of Soil Masses", Chapter 6, *Soil Mechanics: Selected Topics*, I.K., Lee, Editor, Butterworths, 625 p.

den Hoedt, G., 1986, "Creep and Relaxation of Geotextile Fabrics", *Geotextiles and Geomembranes*, Vol. 4, No. 2, pp. 83-92.

Duncan, J.M. and Schaefer, V.R., 1988, "Finite Element Consolidation Analysis of Embankments", *Computers and Geotechnics*, Vol. 6, No. 2, pp. 77-93.

Fowler, J. and Edris, E.V., Jr., 1987, "Fabric Reinforced Embankment Test Section, Plaquemine Parish, Louisiana, USA", *Geotextiles and Geomembranes*, Vol. 6, Nos. 1 to 3, pp. 1-51.

Fritzinger, S.A., 1990, "Subaqueous use of High-Strength Geotextiles", *Proceedings of the Fourth International Conference on Geotextiles, Geomembranes and Related Products,* Balkema, Vol. 1, The Hague, Netherlands, May 1990, pp. 143-148.

Greenwood, J.H. and Myles, B., 1986, "Creep and Stress Relaxation of Geotextiles", *Proceedings of the Third International Conference on Geotextiles*, Vol. 2, Vienna, Austria, April 1986, pp. 821-824.

Greenwood, J.H., 1990, "The Creep of Geotextiles", *Proceedings of the Fourth International Conference on Geotextiles, Geomembranes and Related Products*, Balkema, Vol. 2, The Hague, Netherlands, May 1990, 645-650.

Helwany, M.B. and Wu, J.T.H., 1992, "A Generalized Creep Model for Geosynthetics", *Earth Reinforcement Practice*, Ochiai, H., Hayashi, S., and Otani, J., Editors, Balkema, Vol. 1, Proceedings of the International Symposium on Earth Reinforcement Practice, Kyushu University, Fukuoka, Japan, November 1992, pp. 79-84.

Helwany, M.B. and Wu, J.T.H., 1995, "A Numerical Model for Analyzing Long-Term Performance of Geosynthetic-Reinforced Soil Structures", *Geosynthetics International*, Vol. 2, No. 2, pp. 429-453.

Holtz, R.D., Christopher, B.R., and Berg, R.R., 1997, "*Geosynthetic Engineering*", BiTech Publishers Ltd, Richmond, British Columbia, Canada, 452 p.

Industrial Fabrics Association International, 1999, "2000 Specifier's Guide", *Geotechnical Fabrics Report*, Vol. 10, No. 7, 196 p.

Janbu, N., 1963, "Soil Compressibility as Determined by Oedometer and Triaxial Tests", *Proceedings of the European Conference on Soil Mechanics and Foundation Engineering,* Wiesbaden, Germany, Vol. 1, pp. 19-25.

Jewell, R.A., and Greenwood, J.H., 1988, "Long Term Strength and Safety in Steep Soil Slopes Reinforced by Polymer Materials", *Geotextiles and Geomembranes*, Vol. 7, Nos. 1 to 2, pp. 81-118.

Kabir, M.H., 1988, "Creep Behaviour of Geotextiles", *Theory and Practice of Earth Reinforcement*, Yamanouchi, T., Miura, N., and Ochiai, H., Editors, Balkema, Proceedings of the International Geotechnical Symposium on Theory and Practice of Earth Reinforcement, Fukuoka Kyushu, Japan, October 1988, pp. 111-116.

Koerner, R.M., Hsuan, Y., and Lord, A.E., 1993, "Remaining Technical Barriers to Obtaining General Acceptance of Geosynthetics", *Geotextiles and Geomembranes*, Vol. 12, No. 1, pp. 1-52.

Leshchinsky, D., Dechasakulsom, M., Kaliakin, V.N. and Ling, H.I., 1997, "Creep and stress relaxation of geogrids", *Geosynthetics International*, Vol. 4, No. 5, pp. 463-479.

Leroueil, S. and Rowe, R.K., 2001, "Embankments Over Soft Soil and Peat", *Geotechnical and Geoenvironmental Engineering Handbook,* R.K. Rowe, Editor, Kluwer Academic Publishers, Norwell, Georgia, USA, 1088 p.

Li, A.L., 2000, *"Time Dependent Behaviour of Reinforced Embankments on Soft Foundations*", Ph.D. Thesis, Faculty of Engineering Sciences, The University of Western Ontario, London, Ontario, Canada, 398 p.

Li, A.L. and Rowe, R.K., 2000, "*Reinforced Embankments Constructed with Prefabricated Vertical Drains: Analysis and Implications for Design*", Report No. GEOT-12-00, Faculty of Engineering Science, The University of Western Ontario, London, Ontario, Canada, 60 p.

Ling, H.I., Wu, J.T.H., and Tatsuoka, F., 1992, "Short-Term Strength and Deformation Characteristics of Geotextiles Under Typical Operational Conditions", *Geotextiles and Geomembranes*, Vol. 11, No. 2**,** pp. 185-219.

Litwinowicz, A., Wijeyakulasuriya, C.V., and Brandon, A.N., 1994, "Performance of a Reinforced Embankment on a Sensitive Soft Clay Foundation", *Proceedings of the Fifth International Conference on Geotextiles, Geomembranes and Related Products*, Vol. 1, Singapore, September 1998, pp. 11-16.

Loke, K.H., Ganeshan, V., Werner, G., and Bergado, T.D., 1994, "Composite Behaviour of Geotextile Reinforced Embankment on Soft Clay", *Proceedings of the Fifth International Conference on Geotextiles, Geomembranes and Related Products,* Vol. 1, Singapore, September 1998, pp. 25-28.

Lopes, M.L., Cardoso, A.S., and Yeo, K.C., 1994, "Modelling Performance of a Sloped Reinforced Soil Wall using Creep Function", *Geotextiles and Geomembranes*, Vol. 13, No. 3, pp. 181-197.

McGown, A. Andrawes, K.Z., and Kabir, M.H., 1982, "Load-Extension Testing Geotextiles Confined In-Soil", *Proceedings of the Second International Conference on*

Geotextiles, IFAI, Vol. 3, Las Vegas, Nevada, USA, August 1982, pp. 793-798.

McGown, A., Andrawes, K.Z., Yeo, K.C., and DuBois, D., 1984, "The Load-Strain-Time Behaviour of Tensar Geogrids", *Polymer Grid Reinforcement*, Thomas Telford, 1985, Proceedings of a conference held in London, UK, March 1984, pp. 11-17.

McGown, A., Andrawes, K.Z., Pradhan, S., and Khan, A.J., 1998, "Limit State Design of Geosynthetic Reinforced Soil Structures", *Proceedings of the Sixth International Conference on Geosynthetics*, IFAI, Vol. 2, Atlanta, Georgia, USA, March 1998, pp. 144-179.

Mylleville, B.L.J. and Rowe, R.K., 1988, "*Simplified Undrained Stability Analysis for Use in the Design of Steel Reinforced Embankments on Soft Foundations*", Report No. GEOT-3-88, Faculty of Engineering Science, University of Western Ontario, London, Ontario, Canada, 73 p.

Mylleville, B.L.J. and Rowe, R.K., 1991, "On the Design of Reinforced Embankments on Soft Brittle Clays", *Proceedings of Geosynthetics '91*, IFAI, Vol. 1, Atlanta, Georgia, USA., February 1991, pp. 395-408.

Nothdurft, D.B. and Janardhanam, R., 1994, "Influence of Polymer Viscoelasticity in Reinforced Soil Structure Design", *Proceedings of the Fifth International Conference on Geotextiles, Geomembranes and Related Products*, Vol. 1**,** Singapore, September 1994, pp. 247-250.

Perkins, S.W., 2000. "Constitutive Modeling of Geosynthetics", *Geotextiles and Geomembranes,* Vol. 18, No. 5, pp. 273-292.

Rowe, R.K. and Soderman, K.L., 1985, "An Approximate Method for Estimating the Stability of Geotextile Reinforced Embankments", *Canadian Geotechnical Journal*, Vol. 22, No. 3, pp. 392-398.

Rowe, R.K. and Ho, S.K., 1986, "Determination of Geotextile Stress-Strain Characteristics using a Wide Strip Test", *Proceedings of the Third International Conference on Geotextiles*, Vol. 3, Vienna, Austria, April 1986, pp. 885-890.

Rowe, R.K. and Soderman, K.L., 1987, "Stabilization of Very Soft Soils using High Strength Geosynthetics: The Role of Finite Element Analyses", *Geotextiles and Geomembranes*, Vol. 6, Nos. 1-3, pp. 53-80.

Rowe, R.K. and Li, A.L., 1999, "Reinforced Embankments Over Soft Foundations Under Undrained and Partially Drained Conditions", *Geotextiles and Geomembranes*, Vol. 17, No. 3, pp. 129-146.

Sawicki, A. and Kazimierowicz-Frankowska, K., 1998, "Creep Behaviour of Geosynthetics", *Geotextiles and Geomembranes*, Vol. 16, No. 6, pp. 365-382.

Sawicki, A., 1999, "Creep of Geosynthetic Reinforced Soil Retaining Walls", *Geotextiles and Geomembranes*, Vol. 17, No. 1, pp. 51-65.

Schiffman, R.L., Chen, A. T-F., and Jordan, J.C., 1969, "An Analysis of Consolidation Theories", *Journal of the Soil Mechanics and Foundations Division*, Vol. 95, No. SM1, pp. 285-312.

Schimelfenyg, P., Fowler, J., and Leshchinsky, D., 1990, "Fabric Reinforced Containment Dike, New Bedford Superfund Site", *Proceedings of the Fourth International Conference on Geotextiles and Geomembranes and Related Products*, Vol. 1, The Hague, Netherlands, May 1990, pp. 149-154.

Shrestha, S.C. and Bell. J.R., 1982, "Creep Behavior of Geotextiles Under Sustained Loads", *Proceedings of the Second International Conference on Geotextiles*, IFAI, Vol. 3, Las Vegas, Nevada, USA, August 1982, pp. 769-774.

Soong, T.Y. and Koerner, R.M., 1998, "Modeling and Extrapolation of Creep Behaviour of Geosynthetics", *Proceedings of the Sixth International Conference on Geosynthetics*, IFAI, Vol. 2, Atlanta, Georgia, USA, March 1998, pp. 707-710.

Thornton, J.S., Paulson, J.N., and Sandri, D., 1998, "Conventional and Stepped Isothermal Methods for Characterizing Long Term Creep Strength of Polyester Geogrids", *Proceedings of the Sixth International Conference on Geosynthetics*, IFAI, Vol. 2, Atlanta, Georgia, USA, March 1998, pp. 691-698.

Wrigley, N.E., 1987, "Durability and Long-Term Performance of Tensar Polymer Grids for Soil Reinforcement", *Material Science Technology*, Vol. 3, The Institute of Metals, pp. 161-170

Wrigley, N.E., Austin, R.A., and Harrison, P.E., 1999, "The Long-Term Strength of Geogrid Reinforcement", *Proceedings of Geosynthetics '99*, IFAI, Vol. 2, Boston, Massachusetts, USA, April 1999, pp. 711-721.

Zhang, C. and Moore, I.D., 1997a, "Nonlinear Mechanical Response of High Density Polyethylene, Part II: Uniaxial Constitutive Modeling", *Polymer Engineering and Science*, Vol. 37, No. 2, pp. 414-420.

Zhang, C. and Moore, I.D., 1997b, "Finite Element Modelling of Inelastic Deformation of Ductile Polymers", *Geosynthetics International*, Vol. 4, No. 2, pp. 137-163.

Zienkiewicz, O.C., 1977, "*The Finite Element Method*", Third Edition, McGraw-Hill, New York, New York, USA, 787 p.

NOTATIONS

Basic SI units are given in parentheses.

a_0 = material constant of the viscoelastic model (N/m)

a_1 = material constant of the viscoelastic model (m/N)

C_k = hydraulic conductivity change index (dimensionless)

CR = construction rate (m/month)

c_K = cohesion intercept (Pa)

E = Young's modulus of soil (Pa)

E_0 = stiffness of independent spring (N/m)

E_1 = material constant (dimensionless)

E_i = stiffness of i^{th} Kelvin element (N/m)

e = void ratio (dimensionless)

e_o = reference/initial void ratio (dimensionless)

f_{c1} = partial factor for undrained shear strength (dimensionless)

f_{c2} = partial factor for interface strength (dimensionless)

f_ϕ = partial factor for friction angle (dimensionless)

f_γ = partial factor for bulk unit weight (dimensionless)

G = shear modulus (Pa)

H = embankment height (m)

H_f = embankment failure height (m)

J_2 = second invariant of deviatoric stress tensor (Pa^2)

J_i = isochronous stiffness (N/m)

J_t = stiffness as measured using wide-width tensile tests (N/m)

K = bulk modulus (Pa)

K_s = material constant of the Janbu's model (Pa)

$K_o^{'}$ = coefficient of earth pressure at rest (dimensionless)

k_h = hydraulic conductivity in horizontal direction (m/s)

k_v = hydraulic conductivity in vertical direction (m/s)

k_{vo} = reference hydraulic conductivity (m/s)

l = mean effective stress corresponding to centre of ellipse (Pa)

M = slope of Drucker-Prager failure envelope (dimensionless)

$M_{N/C}$ = slope of Drucker-Prager failure envelope in normally consolidated stress range (dimensionless)

$M_{O/C}$ = slope of Drucker-Prager failure envelope in overconsolidated stress range (dimensionless)

m = material constant of Janbu's model (dimensionless)

n = number of Kevin elements (dimensionless)

OCR = overconsolidation ratio (dimensionless)

R = aspect ratio (dimensionless)

s_{uo} = undrained shear strength at ground surface (Pa)

T = time (s)

T_{ult} = ultimate strength of geosynthetic (Pa)

t = time (seconds)

α = material constant of viscoelastic model (dimensionless)

β = material constant of viscoelastic model (dimensionless)

ε = total strain (dimensionless)

ε^e = elastic strain (dimensionless)

ε^v = viscous strain (dimensionless)

ε_1 = major principal shear strain (dimensionless)

ε_2 = minor principal shear strain (dimensionless)

ε_{all} = allowable reinforcement strain (dimensionless)

ε_f = mobilised reinforcement strain at embankment failure (dimensionless)

ε_v^p = plastic volumetric strain (dimensionless)

ε_i^v = viscous strain of i^{th} Kelvin element (dimensionless)

$\dot{\varepsilon}$ = total strain rate (s^{-1})

$\dot{\varepsilon}^e$ = elastic strain rate (s^{-1})

$\dot{\varepsilon}^v$ = viscous strain rate (s^{-1})

ϕ' = friction angle (degree)

γ = unit weight (N/m^3)

η_i = dashpot viscosity of i^{th} Kelvin element (N/m-s)

κ = slope of e - ln(σ'_m) curve in overconsolidated stress range (recompression index) (dimensionless)

λ = slope of e - ln(σ'_m) curve in normally consolidated stress range (compression index) (dimensionless)

ν' = Poisson's ratio (dimensionless)

σ = tensile load in reinforcement (N/m)

σ_3 = minor principal stress (Pa)

σ_{ij} = stress tensor (Pa)

σ_m = mean stress (Pa)

σ_y = intercept of ellipse with σ'_m axis (Pa)

$\dot{\sigma}$ = tensile loading rate (Pa)

σ_m' = effective mean stress (Pa)
σ_p' = preconsolidation pressure (Pa)
σ_v' = effective vertical stress (Pa)
τ_i = retardation time of i^{th} Kelvin element (s)
τ_1 = material constant (dimensionless)
ψ = dilatancy angle (degree)